Seasonal evolution of the supraglacial drainage network at Humboldt Glacier, North Greenland, between 2016 and 2020

Lauren D. Rawlins[1*], David M. Rippin[1], Andrew J. Sole[2], Stephen J. Livingstone[2], Kang Yang[3]

5   [1]Department of Environment and Geography, University of York, YO10 5NG, UK,
[2]Department of Geography, University of Sheffield, S3 7ND, UK,
[3]School of Geography and Ocean Science, Nanjing University, Nanjing, People's Republic of China

Correspondence to: Lauren D. Rawlins (lauren.rawlins@york.ac.uk)

Abstract. Supraglacial rivers and lakes are important for the routing and storage of surface meltwater during the summer melt

10   season across the Greenland Ice Sheet (GrIS), yet remain poorly mapped and quantified across the northern part of the ice sheet, which is rapidly losing mass. Here we produce, for the first time, a high-resolution record of the supraglacial drainage network (including both rivers and lakes) and its seasonal behaviour at Humboldt Glacier, a wide-outlet glacier draining a large hydrologic catchment (13,488 km^2), spanning the period 2016 to 2020 using 10 m spatial resolution Sentinel-2 imagery. Our results reveal a perennially extensive yet interannually-variable supraglacial network extending from an elevation of 200

15   m a.s.l to a maximum of ~1440 m a.s.l recorded in 2020, with limited development of the network observed in the low melt years of 2017 and 2018. The supraglacial drainage network is shown to cover an area ranging between 965.7 km^2 (2018) and 1566.3 km^2 (2019) at its maximum seasonal extent, with spatial coverage of up to 2685 km^2 recorded during the early phases of the melt season when a slush zone is most prominent. Up-glacier expansion and the development of an efficient supraglacial drainage network as surface runoff increases and the snowline retreats is clearly visible. Preconditioning of the ice surface

20   following a high melt year is also observed, with the earlier widespread exposure of the supraglacial drainage network in 2020 compared to other years; a finding that may become representative with persistent warmer years into the future. Overall, this study provides evidence of a persistent, yet dynamic, supraglacial drainage network at this prominent northern GrIS outlet glacier and advances our understanding of such hydrologic processes, particularly under ongoing climatic warming and enhanced runoff.

1 Introduction

30   The Greenland Ice Sheet (GrIS) has experienced significant mass loss throughout the 21st Century and currently represents the largest single cryospheric component of global sea level rise, contributing an estimated 10.6 ± 0.9 mm since 1992 (IMBIE, 2020). Over the last two decades, GrIS mass loss has become increasingly dominated by surface mass balance (SMB) processes, accounting for 60% of ice loss annually since 1991, with the remainder attributed to dynamical mass losses from marine-terminating glaciers along the ice sheet periphery (van den Broeke et al., 2016). Such SMB losses are being increasingly

35   revealed by the magnitude and spatial extent of seasonal surface melting and runoff (Trusel et al., 2018), attributed to climate-driven atmospheric warming (Hanna et al., 2012; Hanna et al., 2021), summertime atmospheric circulatory behaviour (i.e. Greenland Blocking Index; Hanna et al., 2012; 2021; McLeod et al., 2016; van den Broeke, 2017) and the ongoing expansion (Noël et al., 2019) and darkening (Tedesco et al., 2016; Ryan et al., 2018; 2019; Riihelä et al., 2019) of the bare ice zone. Between 2011 and 2020, runoff was 21% higher than any of the preceding three decades (Slater et al., 2021).

40

Surface runoff is transported by an expansive and complex supraglacial drainage system which is activated during the summer season (Pitcher and Smith, 2019). This drainage system, made up of an ephemeral network of interconnected supraglacial rivers and lakes, transports and stores large volumes of surface meltwater on the ablating ice surface (Rippin and Rawlins, 2021). Such runoff can become intercepted by crevasses and moulins, that provide connections to the ice sheet bed where the

45   timing and delivery of such water has been shown to affect ice velocity (Zwally et al., 2002; Bartholomew et al., 2010; 2012; Hoffman et al., 2011; Sole et al., 2011; Andrews et al., 2014; Nienow et al., 2017). In particular, meltwater delivery into an inefficient subglacial configuration, such as linked cavities (Kamb, 1987) which typically occurs during the early period of the melt season, can temporarily overwhelm the subglacial hydrologic system, increasing water pressure and enhancing subsequent sliding (Andrews et al., 2014; Davidson et al., 2019). In some regions where moulins and crevasses are absent, supraglacial

50   rivers can extend undisturbed for tens of kilometres across the bare ice surface, flowing directly into the proglacial zone (Yang et al., 2019a; Li et al., 2022). Ultimately, much of this meltwater will end up in the ocean, contributing directly to global sea level rise (Pitcher and Smith, 2019).

Whilst many remote sensing studies have examined components of the supraglacial drainage network in-depth across the

55   largest melt producing western and southwestern sections of the GrIS (Smith et al., 2015; Gleason et al., 2016, 2021; Yang et al., 2021), it is only recently that other significant ice sheet sectors have begun to be mapped (Gledhill and Williamson, 2018; Yang et al., 2019a; Schröder et al., 2020; Turton et al., 2021; Lu et al., 2021). Focus has only recently shifted to the rapidly changing northern regions of the GrIS, with evidence of inland expansion of supraglacial lakes observed in north east Greenland (Turton et al., 2021) which align with climate model projections (Leeson et al., 2015) and the existence of a

60   widespread supraglacial network (Lu et al., 2021). This study utilises Sentinel-2 satellite imagery to map the supraglacial drainage network, including both rivers and lakes, on a major northern outlet glacier of the GrIS - Humboldt Glacier

(79°23.86'N, 64°20.60'W), hereby denoted to HG – to examine its seasonal behaviour at high spatial (10 m) and temporal resolution over five consecutive melt years (2016 – 2020).

2 Study Location

65 The drainage basins of outlet glaciers in the northern sector of the GrIS comprise ~14% of the total ice sheet area, with 82% of the northern sector predominately drained by 12 marine-terminating glaciers which together hold a sea level equivalent (SLE) of 93 cm (Mouginot et al., 2019). Since 1990, this sector has experienced some of the most pronounced changes in surface melt and runoff, attributed to the rapid expansion of the ablation (46%) and bare ice (33%) zone at rates twice as fast than in southern Greenland, with this trend expected to continue with ongoing climatic warming (Noël et al., 2019). Of the

70 northern outlet glaciers that drain the GrIS, HG, also known as Sermersuaq Glacier, is the widest marine-terminating outlet glacier (~91 km wide) in Greenland and is responsible for draining ~5% of the ice sheet alone north-westward into the Kane Basin (Hill et al., 2017; Rignot and Kanagaratnam, 2006; Rignot et al., 2021; Fig. 1). Since the late 1990s, HG has experienced rapid rates of retreat (~162 m a^{-1}) attributed to increases in mean summer air temperatures and sea-ice decline (Carr et al., 2015). Holding an ice volume equivalent of 19 cm of sea level rise, HG is the fourth largest Greenland glacial contributor to

75 sea level rise (Rignot et al., 2021) having lost 161 gigatonnes (Gt) since 1972 and 311 km^2 of its area between 2000 and 2010 (Box and Decker, 2011).

Until recently, few glaciological studies had focussed on HG (Joughin, et al., 1996, 1999; Carr et al., 2015; Livingstone et al., 2017; Hill et al., 2017, 2018; Mouginot et al., 2019; Gray, 2021; Rignot et al., 2001, 2021, Hillebrand et al., 2022). Studies

80 that have examined HG identified a distinctive ice velocity divide between the northern and southern sectors (Rignot et al., 2001, 2021; Carr et al., 2015; Fig. 1d); the northern sector has up to four times faster ice flow than the south. In terms of surface hydrology, several studies have noted the presence of supraglacial lakes (SGLs; Joughin et al., 1996; Selmes et al., 2011; Carr et al., 2015), however none to-date have examined the overall drainage system, including both rivers and lakes, in-detail.

85

90
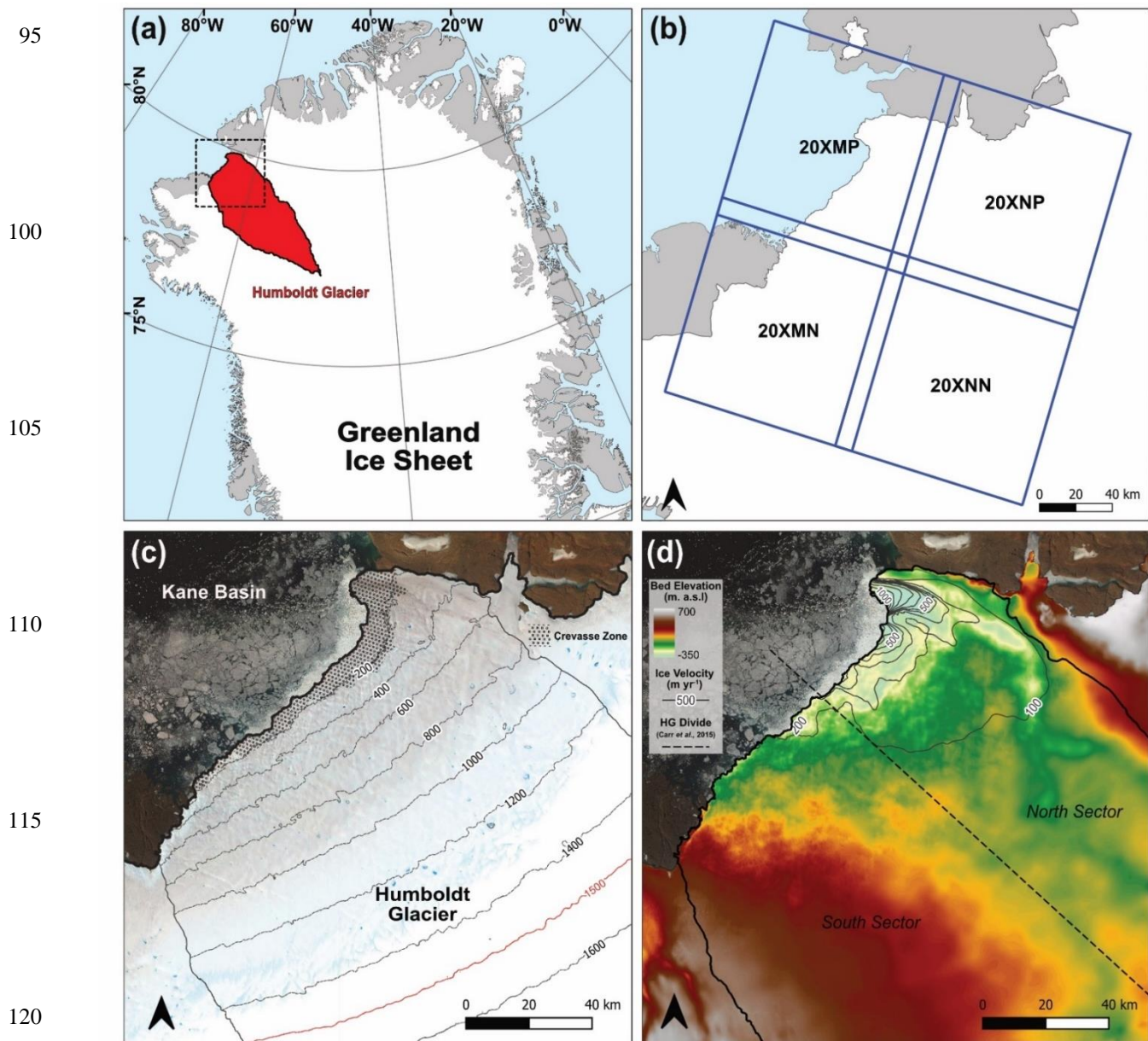
Figure 1. (a) Study location of HG, north Greenland, and its highlighted drainage basin (shaded red). The dashed box shows the inset for other figure boxes (b-d); **(b)** The four Sentinel-2 tiles used for extraction of the supraglacial drainage network across the study region; **(c)** True colour (R: band 4; G: band 3; B: band 2) Sentinel-2 image of HG acquired from 25th July 2020 courtesy of the Copernicus Open Access Hub (https://scihub.copernicus.eu). HG denoted drainage basin and 200 m contour lines derived from ArcticDEM (10 m) are shown. The 1500 m a.s.l contour denotes the maximum melt extent. The shaded section up to 200 m a.s.l also shows the heavily crevassed zone that exists within the northern sector of the terminus; **(d)** Bed topography of HG and the surrounding area from Bed Machine version 4 (Morlighem et al., 2021), ice velocity contours via NASAs MEaSUREs ITS_LIVE project (Gardener et al., 2019) and the division of Humboldt's north and south sectors (dashed line) as per Carr et al. (2015).

3 Data and Methodology

3.1 Data sources

130 Earth-observing satellites enable the study of supraglacial drainage features with broad spatial and temporal coverages (Rennermalm et al., 2013; Yang and Smith, 2012; Chu, 2014). Over the last four decades, the Landsat program has provided a wealth of remotely-sensed data for the mapping and quantification of a number of supraglacial features such as SGLs (Lampkin and Vanderberg, 2011; Pope et al., 2016; Gledhill and Williamson, 2017, 2018; Yang et al., 2019b; Otto et al., 2022), as well as for exploring the generalised configuration (i.e., main river stems) of the supraglacial drainage system

135 (Lampkin and Vanderberg, 2014; Yang et al., 2021). But, its spatial resolution in the visible spectrum (30 m) precludes the reliable delineation of numerous smaller supraglacial rivers (Yang et al., 2019a). This has resulted in these complex networks being unmapped and underrepresented (Chu, 2014). The application of the Multispectral Instrument (MSI) on Sentinel-2 satellites (Sentinel-2A and -2B), which launched in 2015 and 2017 respectively, offers a higher-resolution (10 m) perspective of such systems (Yang et al., 2019a; Lu et al., 2020; Lu et al., 2021). Sentinel-2 imagery enables the detection and delineation

140 of both wide, main-stem river channels, which have high stream orders and are perennially reoccupied (Pitcher and Smith, 2019) as well as narrower (one pixel, or 10 m), tributary-style channels that are lower-order and shallower in depth (Smith et al., 2015; Fig. 2). Sentinel-2 imagery has also been shown to better-resolve supraglacial networks in general for mapping purposes at a glacier-wide scale, particularly in terms of river continuity (Yang et al., 2019a), hence its preferred use in this study.

145

For the years 2016 to 2020, a total of 176 Sentinel-2 Level-1C (orthorectified top-of-atmosphere reflectance) images with sub-pixel multispectral registration (Baillarin et al., 2012) were acquired over HG (Fig. 1b; Table S1) obtained from ESA's Scientific Data Hub (https://scihub.copernicus.eu/dhus/#/home). These images covered the entirety of the study area on forty-four days between the months of May and September across the study period, equating to 1-2 images per month, allowing us

150 to gain a full melt season perspective of supraglacial drainage evolution for the HG drainage catchment. For scenes with cloud cover below a 20% threshold, cloud coverage was typically restricted to the Kane Basin waterway (Fig. 1c) or ice interior locations beyond the melt extent, so did not pose any significant problems for river and lake mapping.

155
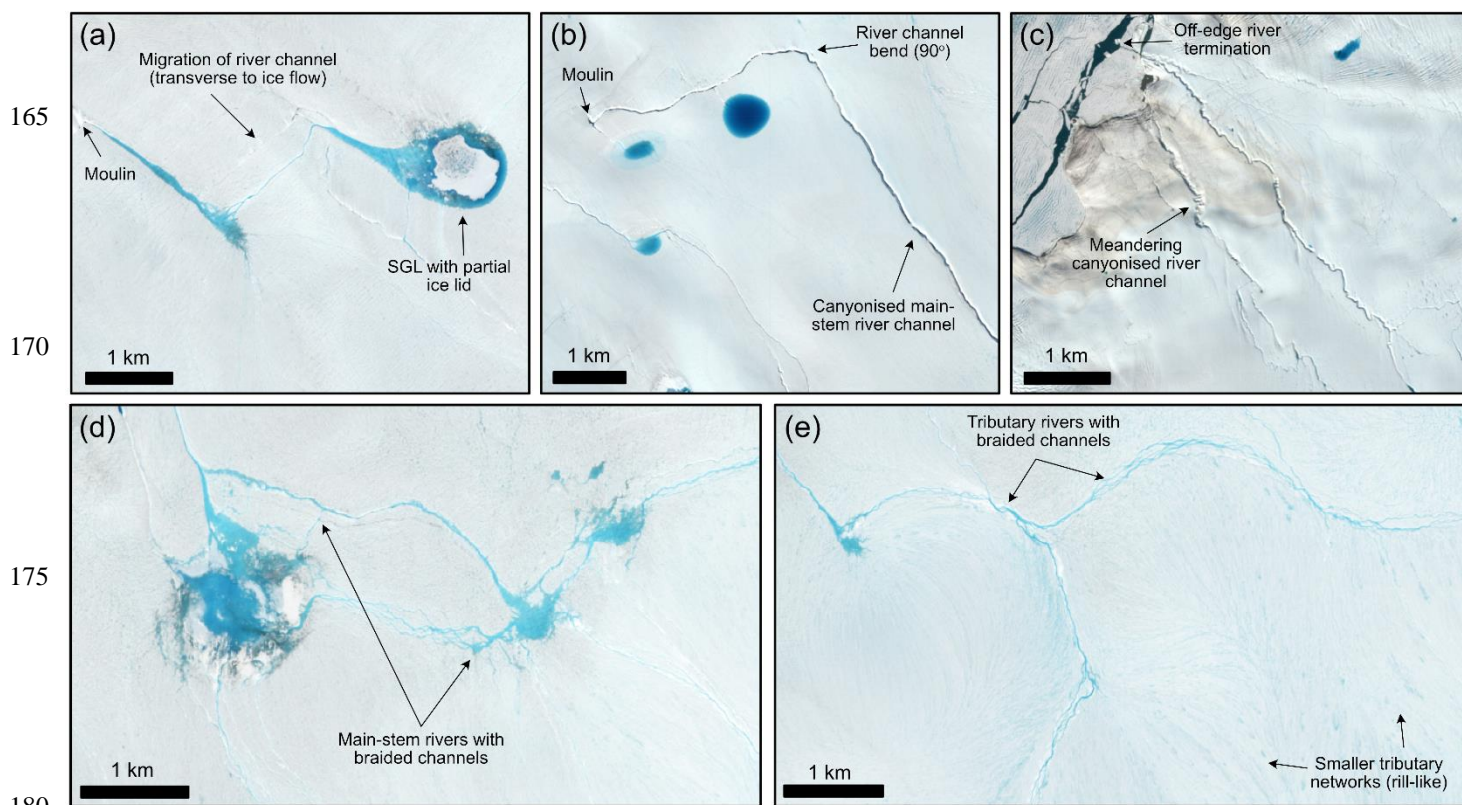
160
Figure 2. Example of the supraglacial drainage features found across the study region of HG from a Sentinel-2 image taken on 23rd June 2020 (RGB). (a) A supraglacial lake with a central ice-lid feeding an outlet supraglacial river, with evidence of river advection transverse to ice flow; (b) a large canyonised supraglacial river with a 90-degree bend terminating abruptly in a moulin; (c) Deep, canyonised supraglacial rivers flowing off the ice edge; (d) Braided supraglacial rivers flowing between supraglacial lakes, known as 'connector' lakes; (e) Narrow supraglacial rivers with rill-features seen in the higher elevation regions of HG, flowing and coalescing into braided tributary rivers. The Sentinel-2 image is courtesy of the Copernicus Open Access Hub (https://scihub.copernicus.eu).

The HG drainage catchment was generated using the ArcticDEM 10 m mosaic product obtained from the Polar Geospatial Centre (https://www.pgc.umn.edu/data/arcticdem/) and delineated following the method of Karlstrom and Yang (2016). Elevation contours at 100 m intervals were defined across the HG basin. Daily surface meltwater production and runoff for the study area were extracted from the Modèle Atmosphérique Régional (MAR) regional climate model (RCM) v3.11 at 6 km resolution (available at ftp://ftp.climato.be/). These data were used to generate estimates of daily meltwater production and runoff (R) in mm water equivalent per day (mm w.e. day^{-1}) within each grid cell to assess the spatial and temporal distribution

of meltwater against mapped supraglacial rivers and lakes. MAR grid cells were also sampled at each 100 m interval to assess
195 elevational gradients in both mapped drainage and runoff.

3.2 Supraglacial river and lake extraction

To effectively delineate supraglacial rivers from remotely sensed imagery, an automatic linear enhancement method developed
by Yang et al. (2015) was used, which characterises supraglacial rivers according to their Gaussian-like brightness cross
sections and longitudinal open channel morphology. Firstly, a Normalised Difference Water Index was performed following
200 McFeeters (1996) to differentiate active surface meltwater from the background ice and snow (Lu et al., 2020; Li et al., 2022).
This equation (Eq.1) utilises Band 3 ('Green') and Band 8 ('NIR') from Sentinel-2 imagery, as follows:

$$NDWI = \frac{(Green - NIR)}{(Green + NIR)} \tag{1}$$

205 Next, an ice mask was applied, created from manually digitising the HG terminus from the latest, end-of-season image (late-
August/early-September) in each of the study years, to extract ice-only regions and remove surrounding land, rocky outcrops
and the ocean of the Kane Basin. A separate crevasse mask was delineated from manually identifying the heavily crevassed
zone known to extend up to 25 km from the northern sector of the terminus, with particular prevalence across the 7 km floating
section (Carr et al., 2015). This mask was used to avoid the erroneous delineation of crevasses and crevasse shadows in this
210 area during image processing, as well as to reduce the effects of drainage overestimation in these ice marginal regions in further
calculations (Ignéczi et al., 2018). A high-value, global NDWI threshold (t_{ndwi} = 0.4) was then applied to the masked NDWI
image to extract SGLs and wide, main-stem river segments. To aid in delineating narrower river segments and obtain a
complete and continual supraglacial network, the automatic river detection algorithm for linear enhancement (Yang et al.,
2015) was then applied. This involved the removal of the low-frequency image background and high-frequency image noise
215 using a band-pass filter ramped between 1/200 m⁻¹ and 1/40 m⁻¹ (Yang et al., 2019a), before the application of a Gabor filter
to enhance the cross sections of smaller rivers (<2-pixel width). This was followed by a parsimonious path opening (PPO)
operator, which is a flexible mathematical morphological operator, to stabilise linear brightness across river lengths and
preserve connectivity, with a minimum path length of 20 pixels.

220 After Gabor-PPO filtering, the supraglacial river network becomes easier to differentiate and delineate from the surrounding
icy background. A global pixel brightness threshold of 5 (out of 255) denoted t^5, was used to extract supraglacial rivers of
varying widths from Gabor-PPO opened filtered images (Lu et al., 2020), i.e., from tributary-style rivers to main-stem, large
river channels. Hydrologically-connected saturated slush zones were retained as they play an important role in the initial
mobilisation and inland expansion of the melt zone as summer progresses (Marston, 1983; Cuffey and Paterson, 2010; Chu,
225 2014; Rippin and Rawlins, 2021). Whilst dynamic thresholding techniques have been used in other studies, particularly in the

identification and mapping of supraglacial lakes across independent dates and/or years (Selmes et al., 2011; Williamson et al., 2017), applying these two separate thresholds (t_{ndwi} and t^5) to all images across this study period is reasonable for exploring the seasonal behaviour over the available dates used. Finally, these masks were vectorised into separate river channel polylines and lake polygons for analysis, with a size threshold of 0.1 km^2 applied to SGLs.

3.3 Supraglacial river and lake quantification

To characterise the extracted supraglacial drainage system, metrics were calculated for both rivers and lakes. These metrics are summarised in Table S2 and include meltwater area (km^2), meltwater area fraction (MF, %), the number of supraglacial lakes (L_n) and supraglacial lake area (L_a). MF is defined as the percentage total meltwater area across the drainage catchment below the maximum extent elevation of 1500 m a.s.l for each date mapped, which is then also further divided into separate feature ratios including river fraction (RF) and lake fraction (LF). MF was also calculated across 100 m elevation contours from above the heavily crevassed zone at 200 m a.s.l, to the maximum melt extent at 1500 m a.s.l. To explore the relationship between remotely-mapped drainage and modelled RCM MAR runoff (R), a Spearman's rank correlation (r_s) was performed and linear regression analysis undertaken with subsequent R^2, r_s and *P*-values reported.

4 Results

4.1 Spatial characteristics of the supraglacial drainage network

Supraglacial rivers and lakes were mapped from a total of forty-four dates across the 13,488 km^2 HG drainage basin up to a maximum melt extent of 1500 m a.s.l from the melt seasons of 2016 to 2020. The mapped supraglacial drainage network across HG is shown extend up to 1500 m a.s.l, with well-developed, main-stem river channels occurring up to 1000 m a.s.l, which we characterise as the persistent zone, and an ephemeral network of tributary-style rivers and slush zones extending beyond 1000 m a.s.l in a transient zone up to maximum extent (Fig. 3a). Active supraglacial rivers and lakes form progressively up-glacier from low elevations (200 m a.s.l) to a maximum of 1440 m a.s.l as the melt seasons progress across the study period, with interannual variability observed.

Within the lower elevation regions (<400 m a.s.l) of HG, collectively the supraglacial drainage network is largely fragmented, with many short (<750 m long), supraglacial rivers observed alongside small SGLs with an average size of 0.23 km^2: the smallest observed across all elevation bands. At greater elevations, beyond 400 m a.s.l, we observe large, main-stem supraglacial rivers, some with incised-canyon features (Fig. 2b), interconnected with increasingly larger SGLs. SGLs and rivers parallel to ice flow tend to be highly persistent year-on-year across the study period. In Figure 3b, we also see some evidence of a potential main-river reconfigurations, with the north-westward advection of a river channel that runs transverse to ice flow. In the upper parts of the catchment, the supraglacial drainage network becomes increasingly dense, especially between 800 – 1000 m a.s.l, where we see a 120% increase in average meltwater area (94.5 km^2) compared to 200 – 400 m

a.s.l (42.9 km^2), a 79% increase compared to 400 – 600 m a.s.l (54.2 km^2) and a 10% increase compared to 600 – 800 m a.s.l. Not only are persistent main-stem rivers still present up to 1000 m a.s.l, but an extensively connected tributary river system is also observed within this persistent zone.

260
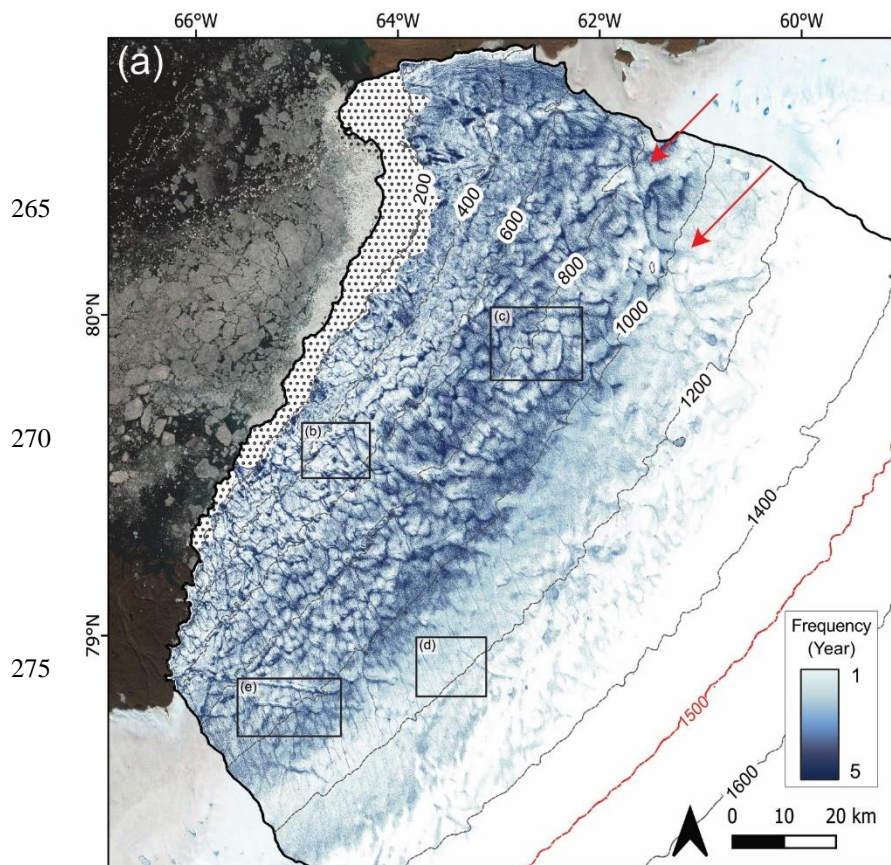
265

270

275

280

285

290
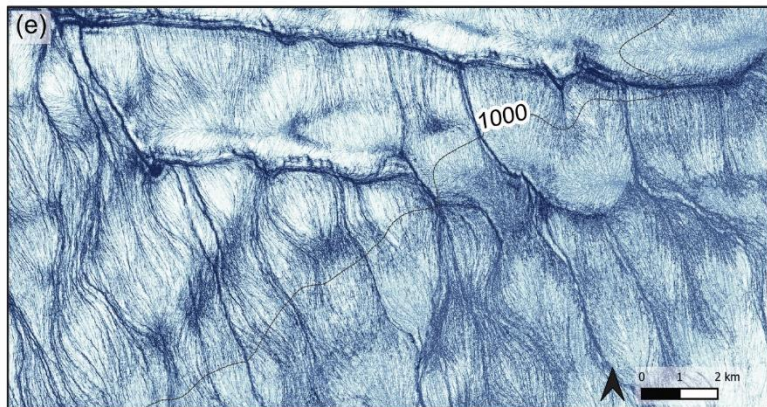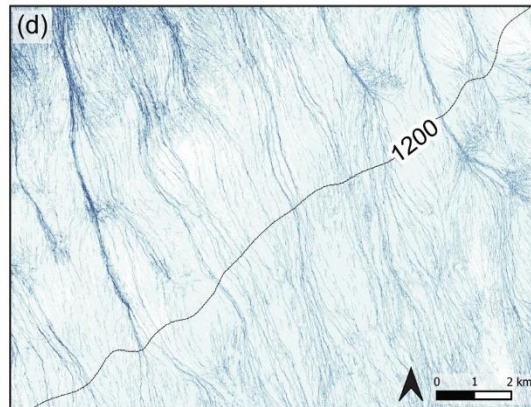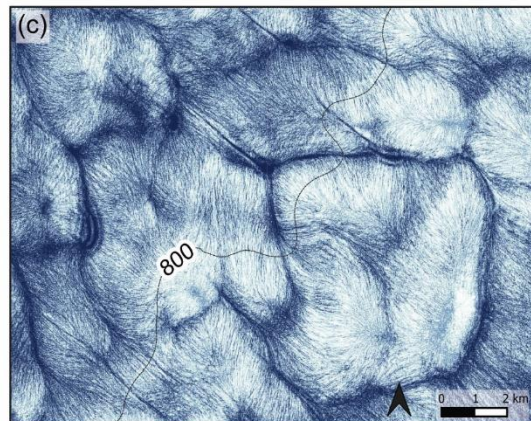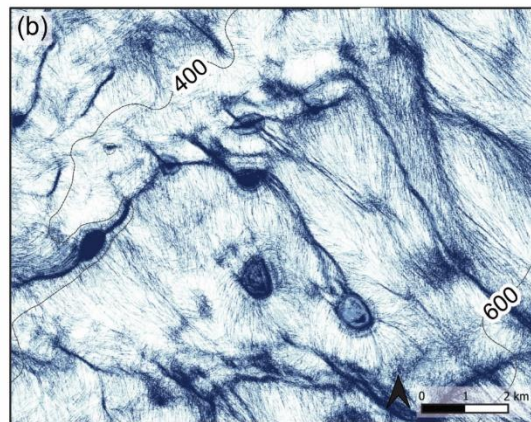
Figure 3. – (a) Map showing the recurrence frequency of the supraglacial drainage system across the study period (2016 to 2020) at HG. Dark blue shades denote a higher frequency of return, which is highly prominent in the persistent zone below 1000 m a.s.l, with rivers and lakes typically reforming in the same location each year. Red arrows denote the location and direction of two distinct parallel drainage structures. The background Sentinel-2 image courtesy of the Copernicus Open Access Hub (https://scihub.copernicus.eu); (b) close-up panel showing highly persistent rivers in the persistent zone with a prominent 90-degree angle in their channel form; (c) close-up panel showing the dendritic supraglacial drainage structure typical in the northern sector of HG; (d) close-up panel of the transient zone (> 1000 m a.s.l) where yearly river persistence is lower and characterised by lengthy tributary river channels; (e) close-up panel showing the more parallel-form of supraglacial drainage structure in the southern sector of HG.

The drainage network up to 1000 m a.s.l, in particular within the central and northern reaches of HG, is dendritic in nature (Fig. 3c). This type of drainage, however, is not uniform across HG, with the supraglacial network to the south exhibiting a more sub-parallel drainage style (Fig. 3e), with this configuration extending beyond the persistent zone and into the more transient zone with slush zone development and inland evolution a key part of the temporal aspect of the network at higher elevations (Fig. 3a). Even though density remains high until 1300 m a.s.l, vastly transient tributary rivers and slush zones dominate, feeding meltwater from headwater regions downstream. In terms of SGLs, the maximum recorded elevation was 1346 m a.s.l both in 2019 and 2020. Fewer SGLs are observed in the transient zone, accounting for 16% of total SGL area across the study period. However, average SGL area increases with elevation, with lakes in this zone being 54% larger (0.4 km^2) on average than those found below 1000 m a.s.l (0.26 km^2). The single largest SGL size of 2.08 km^2 was recorded in 2016 at 1150 m a.s.l.

A key feature that is particularly prominent in the supraglacial drainage network is the presence of two parallel lines that track across-glacier from a south-west to north-east direction (Fig 3a). Many supraglacial rivers and lakes are aligned along these two features, including the abrupt termination of many rivers, indicating a strong structural element here which influences drainage configuration.

4.2 Temporal evolution of the supraglacial drainage network

Typically, the supraglacial drainage network becomes active in early-June with the on-set of melt production and runoff in the region, with only a small number of large-stem supraglacial rivers becoming active and subsequently recorded (MF <3.2%) during this time within the mapped elevation bands of 200 – 950 m a.s.l. By late June a widespread (500 m to 1150 m a.s.l) slush zone develops and advances up-glacier as the melt season progresses runoff increases, with MF ranging between 11.4 and 19.9%. As bare ice is exposed below this slush zone, the drainage system becomes increasingly channelised (Fig. 4). The formation of the slush zone at the end of June typically coincides with maximum melt storage in SGLs (both numbers and size of lakes). The largest slush zone and number of SGLs in this study was observed on 30th June 2019 (Fig. 4), with 2685 km^2

(19.9%) of the HG ice surface comprised of a hydrologically-connected, unchannelised system and 111 SGLs recorded (total
325 area 27.4 km^2). As the season progresses, the slush zone shifts upglacier whilst reducing in size, with average June MF
decreasing by up to 33% before stagnating at a maximum inland extent, ranging between 1050 m a.s.l (2018) and 1440 m a.s.l
(2020) across the study period. At this elevation, the slush zone operates as headwaters, feeding the complex, transient,
tributary systems below and further suppling the larger, well-defined supraglacial rivers at lower elevations (<1000 m a.s.l).

330 Towards the end of the melt season, despite melt and runoff cessation, the supraglacial drainage network remains (Fig. 4).
The interannual variability in seasonal behaviour of the supraglacial drainage network between 2016 and 2020 (Fig. 4)
corresponds to the length and intensity of the melt season. Drainage within the melt seasons of 2016, 2019 and 2020 follow a
similar pattern characterised by a rapid increase and peak in MF in late-June, yielding values of 11.4% (R = 7.1 mm day^{-1}),
19.9% (R = 19.4 mm day^{-1}) and 12.1% (R = 19.6 mm day^{-1}) respectively (Fig. 5); concurrent with early-season melt production
335 and runoff. These high MF values are largely associated with widespread slush zone initiation, with a subsequent peak in MF
increasing the drainage network area by 267% in 2016 (28th June) and 322% in 2019 (30th June), with its spatial extent observed
below 1000 m a.s.l at this time (Figure S1). The beginning of the melt season in 2020 is an exception, with an anomalously
high MF (11.6%) recorded on the 15th June reaching 1100 m a.s.l, as well as a high number (57) and cumulative area of SGLs
(11.2 km^2; Fig. 5). This high is followed by a 66% reduction in MF by the 23rd June, after which the networks behaviour is
340 similar to that of other seasons, with a subsequent MF increase of 211% to its peak at the end of June (28th June; Fig. 5).
Despite high rates of melt production and runoff throughout July across these three melt seasons, MF plateaus and reduces,
reaching a steady-state of between 7.6% and 13.9%. The number of SGLs also reduces on average between 20% and 27%
throughout July, with cumulative SGL area reducing between 9% and 38%.

345 By the end of July, the supraglacial drainage network consistently extends to 75 - 80 km inland (1440 m a.s.l) at its maximum
areal extent. As melt and runoff reaches declines into August, the drainage network reduces between 53% (2016) and 9%
(2020). In 2019, persistent high rates of melt production and runoff result in persistence of the drainage networks maximum
inland extent and even a late-season increase of 54% in MF from the 5th August to 13th August. 2019 is registered as an
exceptional year at HG, with an average meltwater area up to 75% greater in June compared to 2016, between 25% and 92%
350 greater in July compared to 2016 and 2020 and up to three times greater (300%) in August compared to both 2016 and 2020.
Additionally, 129% and 86% more lakes are recorded compared to 2016 and 2020 respectively, with SGLs persisting much
later into the melt season (mid-August) than the other years.

The supraglacial drainage network in 2017 and 2018 behaves quite differently to the other melt years (Fig S2). Until late-July,
355 MF remains low (<7%; Fig. 5) with runoff predominately occurring within the lower 700 m of the HG basin (Figure S1). The
number and area of SGLs is also low during this period, with an average of 15 lakes observed in June and July across 2017
and 2018 with a cumulative average area of 21.5 km^2 and 31.1 km^2 respectively; 280% lower than average lake counts and

218% lower than cumulative average area for the same monthly periods across 2016, 2019 and 2020. Unlike the other study years, peak MF does not occur until much later in the melt season, reaching 10.2% on 22nd August 2017 and 7.2% on 20th
360 August 2018 with a 690 km^2 (197%) and 521 km^2 (135%) increase in meltwater area to its prior mapped date respectively; concurrent with peak runoff and the widespread occurrence of a late slush zone. Similarly, SGL numbers and area also peak on these dates, with 54 (15.8 km^2) and 74 (20 km^2) lakes recorded, comprising 32% and 39% of total lakes recorded per year respectively. Examination of the maximum extent of the supraglacial drainage network is also revealed to be limited, with a maximum elevation of ~1150 m in 2017 and ~1050 m in 2018, equivalent to between 48 and 51 km inland.

365

When comparing what could be considered as high vs low melt year seasonal patterns, the supraglacial drainage network is twice as large during high melt years (2016, 2019 and 2020) and is seen to form at elevations ~300 m higher than in low melt years (2017, 2018; Fig. S2). In terms of the average number of SGLs, there is almost double the number of SGLs observed (92%) in the high melt years compared to low melt years with average SGL area also being 111% higher, showing large year-
370 on-year variability of this system. On average, the contribution of supraglacial rivers to peak meltwater area fraction is 98% across all study years, with supraglacial lakes playing a less dominant role in HG's drainage network (Figure S3).

375

380

385

390
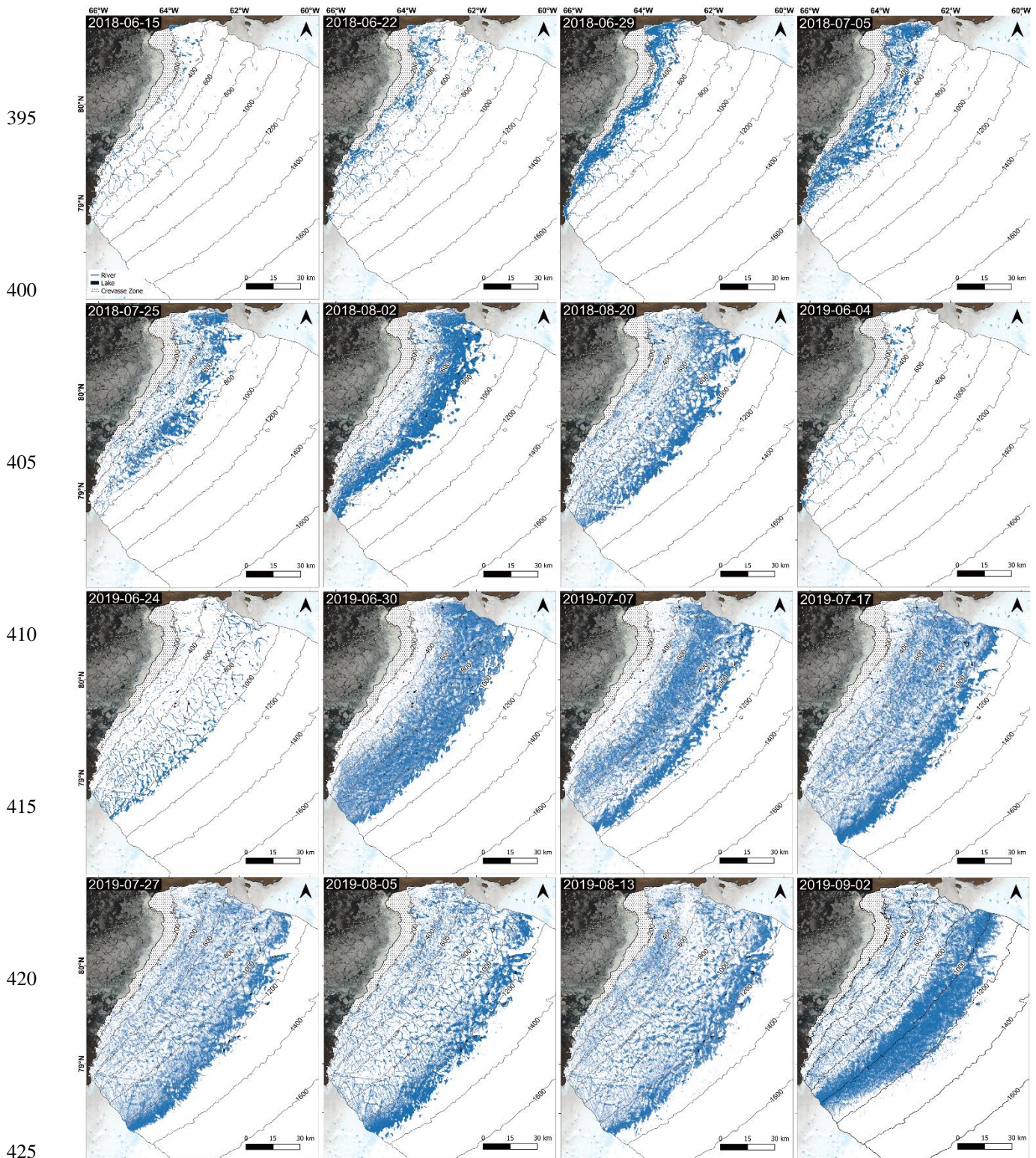
Figure 4. Satellite-derived mapping of the temporal evolution of the supraglacial drainage network, including rivers and lakes, across the HG drainage basin from two melt years during the study period; 2018 showing the typical behaviour of a low melt year and 2019 showing the behaviour during a high melt year. The background image is a Sentinel-2 image courtesy of the Copernicus Open Access Hub (https://scihub.copernicus.eu). For all mapped study dates, please refer to Fig. S2.

430

435

440

445

450
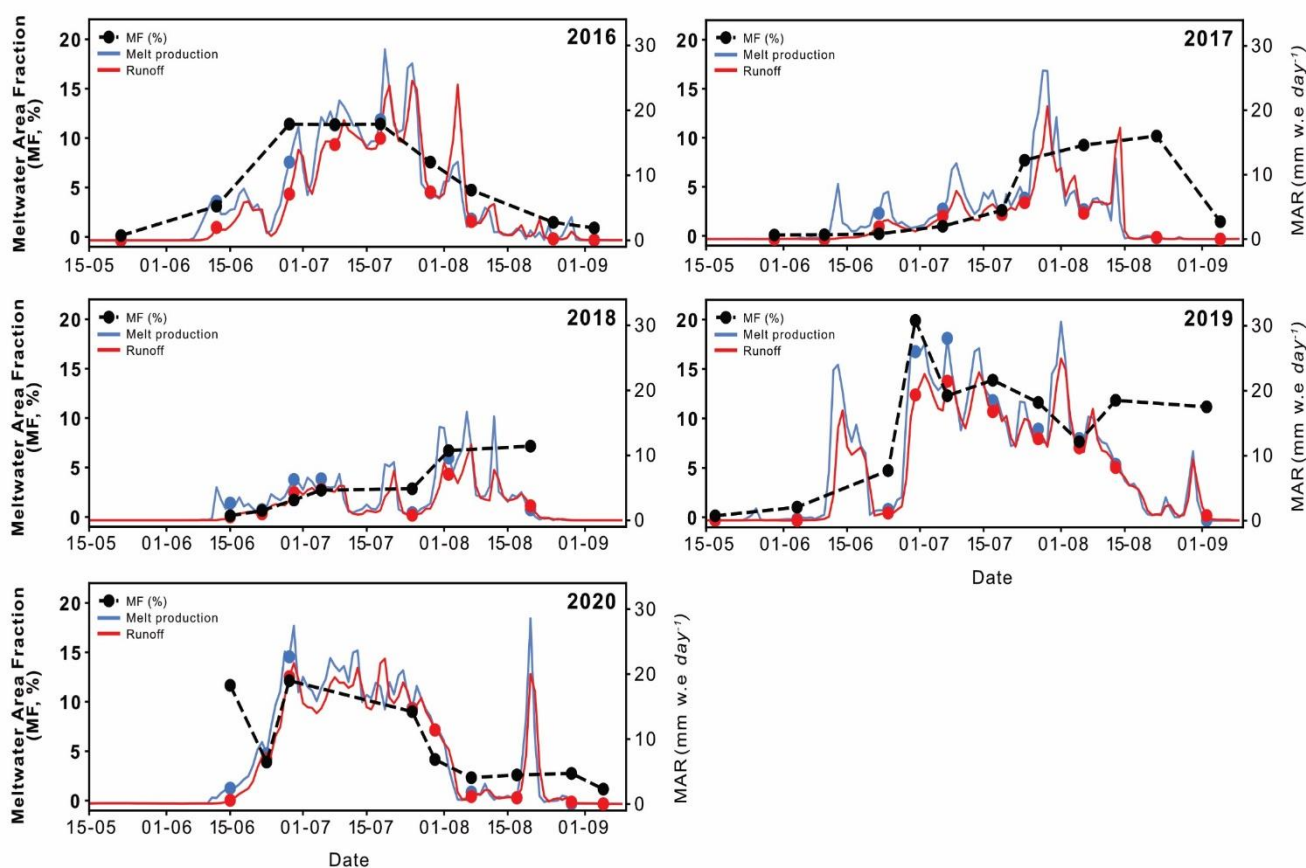
Figure 5. The satellite-derived water metric meltwater area fraction (MF, %) for each mapped date across the study period alongside MAR v3.11 derived melt production and runoff values (mm w.e day^{-1}) for the HG catchment.

455

4.3 Supraglacial hydrology and MAR runoff

A strong positive linear relationship was identified between satellite-derived MF and regional climate model MAR surface R
460   for the HG catchment across the study period 2016 to 2020 (Figure 6: R^2 = 0.77, R_s = 0.91, p = <0.001) up until peak MF
values and rapid surface runoff decline at the end of the melt season. Both MF and R increased concurrently each year as the
melt season progressed, with peak runoff often coinciding with the existence of expansive slush fields across the upper part of
the catchment. Runoff remained high until maximum extent occurred, particularly for high melt years: 2016 (29th July, R =
7.5 mm day^{-1}), 2019 (13th August, R = 8.2 mm day^{-1}) and 2020 (30th July, R = 11.4 mm day^{-1}). For low melt years, runoff
465   remained relatively high until early August (6th August 2017, R = 4.0 mm day^{-1}; 2nd August 2018, R = 7.1 mm day^{-1}), with
maximum extent occurring within two-weeks (the next mapped date). This relationship between MF and R shows the reliability
of simulated variations in seasonal surface meltwater runoff in capturing the behaviour of the supraglacial drainage network
via satellite-derived water metrics, particularly during high melt years and until runoff declines each melt season.
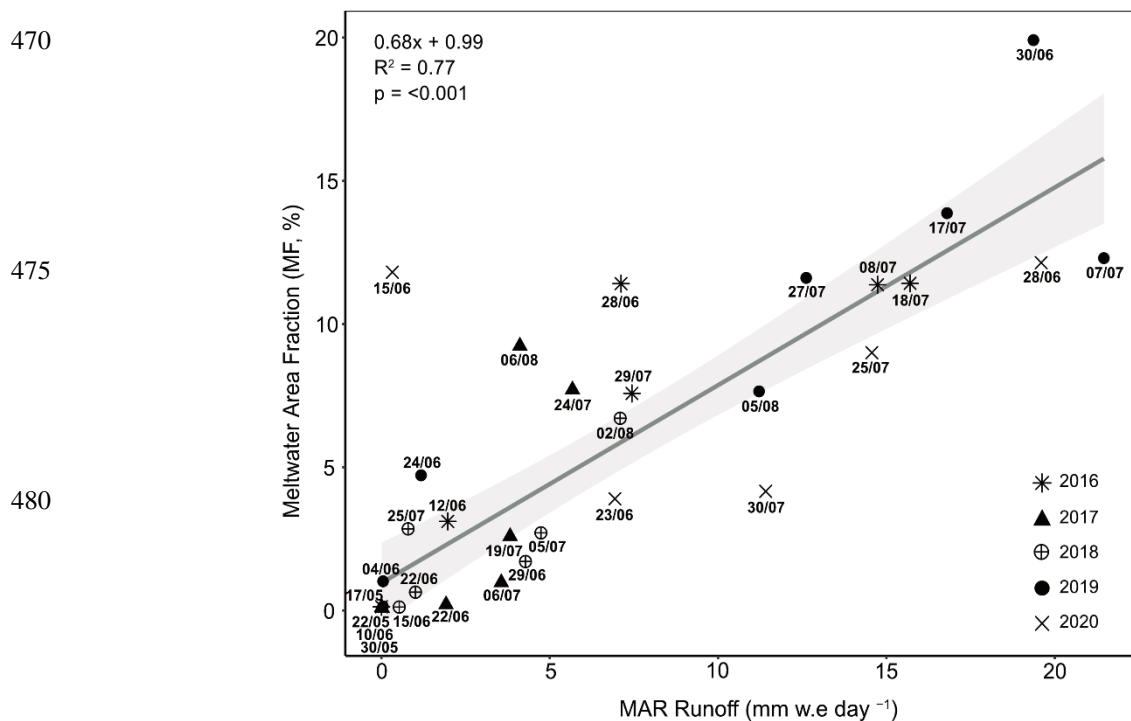
Figure 6. Linear relationship between the satellite-derived water metric meltwater area fraction (MF, %) and RCM-derived runoff from MAR v3.11 for each year studied up until runoff declines.

5 Discussion

5.1 Spatial characteristics of the supraglacial drainage network

Our satellite-derived mapping at HG reveals a complex supraglacial drainage network that is persistent up to 1000 m a.s.l across the study period, with a highly variable system beyond this elevation observed within the transient zone; defined in this study as a high elevation region whereby drainage is transient in time, but not necessarily space. The recurrence frequency of meltwater pixels in the supraglacial drainage network (Fig. 3) demonstrates that SGLs are stable between study years, re-occupying the same location year-on-year despite ice advection (Smith et al., 2015; Pitcher and Smith, 2019). Whilst SGL location is known to be largely controlled by bed topography (Lampkin and Vanderberg, 2011; Igneczi et al., 2018), this study also notes that many well-established rivers that are longitudinal to ice flow, including many with canyonised features, also reoccupy locations. Supraglacial rivers that are transverse to ice flow or have a transverse element to their channel, however, may be less stable in some areas by up ~300 m (Fig. 3a) over the study period, probably due to the impact of ice advection. In the transient zone, the recurrence frequency is reduced, with tributary rivers and slush zones dominating at higher elevations. Here, their persistence is highly reliant on there being enough melt at higher elevations to initiate and sustain channel formation, which in 2017 and 2018, was limited and therefore drainage occurrence was much reduced in this zone. Also, tributary rivers are typically lower order with narrower channels and shallower depths (Smith et al., 2015; Pitcher and Smith, 2019), meaning their form has the potential to migrate, close and reform quickly, if melt is available. The transient zone therefore is not only influenced by melt availability overtime, but the potential for migration in space. In agreement with previous studies (Joughin et al., 2013; Poinar et al., 2015), we also show that rivers tend to be longer at higher elevations (>25 km), likely due to the basal transfer of only long-wavelength basal undulations to the surface due to thicker ice and the reduced presence of surface crevassing (Gudmundsson, 2003; Lampkin and Vanderberg, 2011; Crozier et al., 2018).

Drainage patterns are also shown to vary across HG, with a dendritic-style of drainage observed in the northern sector and a parallel-style drainage observed in the southern sector. These differing patterns not only highlight variations across different hydrologic catchments of the GrIS, but also intra-catchment variations, which may stem from local variations in surface topography via the transmission of basal topography (Raymond and Gudmundsson, 2005; Ng et al., 2018) controlled by wavelength transfer and differing ice flow regimes (Gudmundsson et al., 1998,2003; Lampkin and VanderBerg, 2011; Crozier et al., 2018; Igneczi et al., 2018). This has been shown to play an important role in mapped rivers and lake hydromorphology at both 79°N Glacier (Lu et al., 2021) and across the Devon Ice Cap (Wyatt and Sharp, 2015).

In the northern sector of HG, we observed short supraglacial rivers and small SGLs at lower elevations (200 - 400 m a.s.l) and a prominent dendritic-style drainage pattern of interconnected rivers and lakes up to 1000 m a.s.l, with some larger rivers abruptly terminating. Such characteristics suggest the interception of runoff by crevasses and moulins, with such capture directed to the en- and sub-glacial system with the potential for pronounced impacts on localised flow rates (Catania et al.,

2008; Schoof, 2010; Mejia et al., 2022). As shown by Carr et al. (2015) and Rignot et al. (2021), this sector of HG sits within a 475 m deep basal trough that extends ~45 km wide and >70 km inland and is characterised by fast rates of flow (200 – 600 m yr^{-1}). Faster basal sliding has the ability to promote the more efficient transfer of basal topography to the surface and can subsequently precondition the large-scale spatial structure of the surface drainage system (Crozier et al., 2018; Igneczi et al., 2018).

In comparison, the sub-parallel drainage structure of the supraglacial network in the southern sector largely consists of continuously-flowing rivers that drain surface meltwater from the slush zone at ~1500 m a.s.l to much lower elevations (200 m a.s.l), with some rivers directly terminating off the ice sheet, suggesting limited opportunities for meltwater to penetrate to the ice sheet bed. Similar drainage hydromorphology was also mapped at the neighbouring glacier at Inglefield Land (Yang et al., 2019a; Li et al., 2022), with supraglacial rivers flowing uninterrupted into the proglacial zone. Within this southern sector of HG, ice velocity is significantly slower (<100 m yr^{-1}; Rignot et al., 2021) than its northern counterpart, with relatively thick, broadly impermeable ice contributing to the absence of crevasses and moulins (Oswald and Gogineni, 2011; Yang et al., 2019a; Andrews et al., 2022), as well as controlling the hydromorphology of the drainage network found here.

The supraglacial drainage configuration is also further influenced by significant structural elements which were identified by Livingstone et al., (2017) via the Moderate-Resolution Imaging Spectroradiometer (MODIS) mosaic of Greenland (Haran et al., 2013). Two linear structures that run in a southwest to northeast direction across HG are clearly visible on the mapped glacier surface in this study (Fig 3a, Fig 7), with many supraglacial rivers and SGLs aligned-to or terminating at them. Some longitudinal rivers are also shown to suddenly change direction when encountering these structures, with subsequent channels diverting at a 90-degree angle, transverse to ice flow (Fig. 3a, 3b). It is at the intersection of such structures we observe some channel advection with spacing of 300 m (Fig. 3a), broadly representing the ice displacement over the study period. Other basal structures are also reflected within the supraglacial drainage system, including many V- and X- shaped patterns clearly controlled by depressions in the bed. There is a strong glacier-wide emphasis here of these structures influential control on drainage, which are reproduced here in Figure 7 based on Livingstone et al. (2017) from MODIS imagery (MOG2015, Haran et al., 2018) and also within bed topography data from BedMachine (version 4; Morlighem et al., 2017, 2021). This identification provides independent confirmation of the existence of these depressions in the bed and their subsequent expression on the surface, as well as how they significantly control the multi-year surface drainage configuration within the vicinity of such structures.
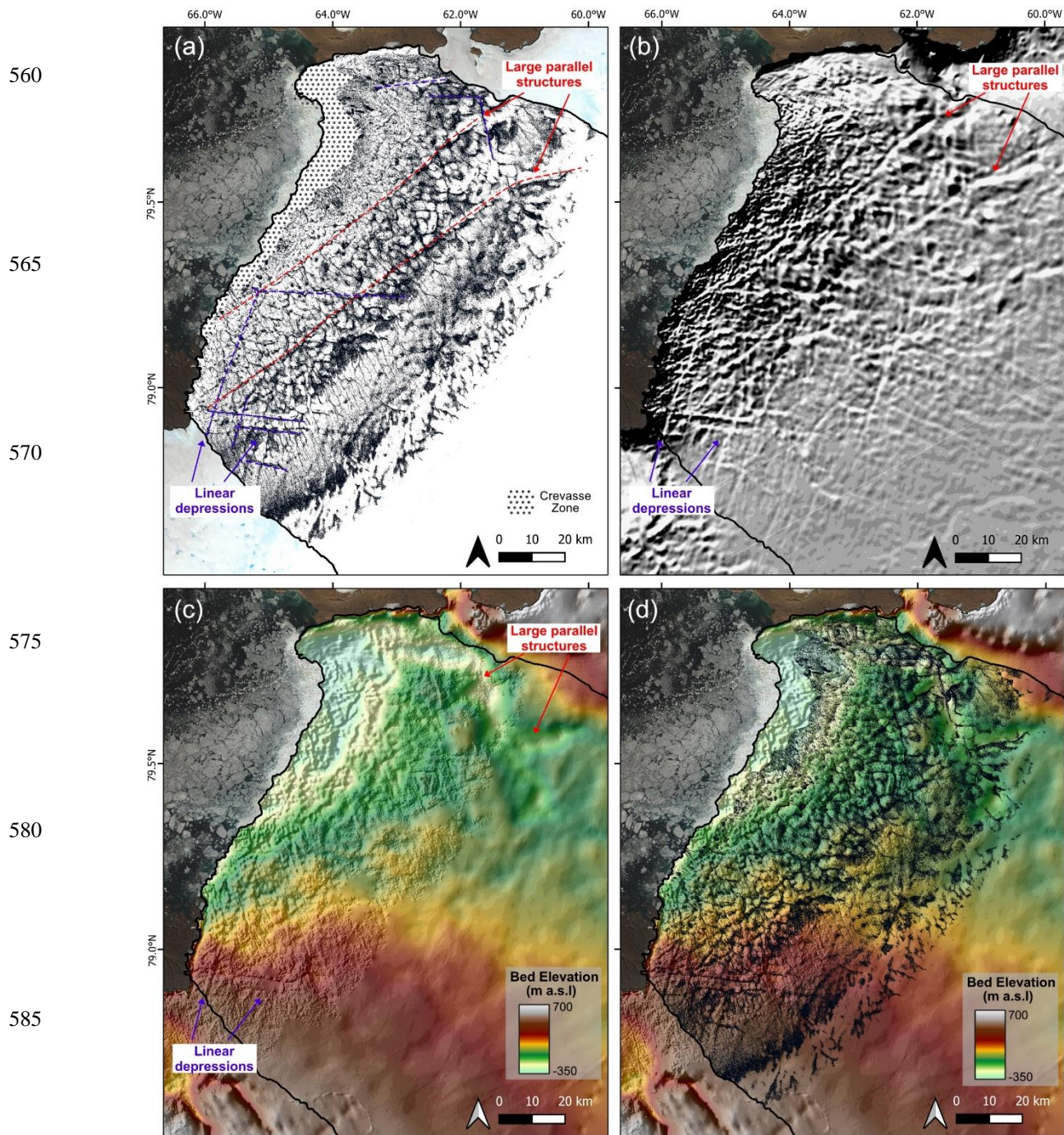
555

**Figure 7. (a) Combined map of the supraglacial drainage network at its maximum extent across 2016 to 2020
showing the two parallel structures orientated southwest to northeast identified by red dashed lines. Other V- and
X-shaped structures in the drainage network are also highlighted by purple dashed lines; (b) Moderate-Resolution
Imaging Spectroradiometer (MODIS) Mosaic of Greenland (MOG2015, Haran et al., 2018) showing evidence of the
these structures on the ice surface; (c) Bed topography via BedMachine (Morlighem et al., 2020) showing the
structures as depressions within the bed; (d) the supraglacial drainage network as presented in (a) overlain on top
of bed topography presented in (c) showing the overall influence bed topography has on the surface drainage
structure at HG.**

595

600

5.2 Temporal evolution of the supraglacial drainage network

Across the study period (2016 – 2020), we observe the seasonal development and inland evolution of the supraglacial drainage
network as the melt season progresses and runoff increases up to the maximum melt extent, which typically occurs at the end-
of-July. During the early melt season and at higher elevations as melt progresses, we observe the growth and inland migration
605 of a large, poorly channelised slush zone (Greuell and Knap, 2000). Within this zone, slush flows can occur as surface melt
percolates and saturates the snowpack, promoting slush mobilisation into topographical lows and initiating the reopening of
perennially-occupied channels (Cuffey and Paterson, 2010; Irvine-Fynn et al. 2011). On higher-draining slopes, such
mobilisation can form slush-filled rills, which coalesce into networks of arborescent tributary channels, efficiently transporting
melt to larger, primary river channels and, subsequently, the transportation of melt down-glacier (Marston, 1983; Cuffey and
610 Paterson, 2010; Chu, 2014; Rippin and Rawlins, 2021). The seasonal development of the drainage network is shown to
transform from a system initially dominated by water percolation to one dominated by channelised, efficient flow (Fig. 4);
further confirming behaviour identified across multiple supraglacial drainage mapping studies across the GrIS (Lu et al., 2021;
Yang et al., 2021; Li et al., 2022).

615 The rate and extent of the spatial and temporal evolution of the supraglacial drainage network is highly variable between years.
Several years within the last decade have been characterised by high air temperatures and extreme melt events, including two
years represented within this study; 2016 and 2019. Both years, in particular 2019, experienced a strong negative North Atlantic
Oscillation and simultaneously a positive East Atlantic index and Greenland Blocking Index phase, which are associated with
persistent, anticyclonic conditions over Greenland driving enhanced surface mass loss (Lim et al., 2016; Cullather et al., 2020;
620 Zhang et al., 2022). Mass loss during 2019, in particular, was promoted by enhanced solar radiation, reduced cloud cover and
the north-westward advection of warm, moist air from the western margins as a result of such atmospheric variability (Hanna
et al., 2021; Cullather et al., 2020; Tedesco and Fettweis, 2020; Elmes, 2021). Combined with low snow accumulation in the
2018/19 winter (Sasgen et al., 2020), extensive melting occurred along much of the Greenland coast, with surface melt

experienced in the north being the highest on the record since 1948 (Tedesco and Fettweis, 2020). It was during this exceptional

625 and long melt year that we observed the highest MF values (19.9% or 2685 km^2 recorded on the 30th June 2019) and second

highest areal extent of supraglacial drainage network (1375 m a.s.l; Fig. 4). Ablation continued throughout September (Sasgen

et al., 2020; Tedesco et al., 2019; Tedesco and Fettweis, 2020), however this was beyond our mapped timeframe. The year

2019 also recorded the largest number of SGLs (527) and cumulative lake areas (151.8 km^2). The hydrologic expansion of the

drainage network was also rapid, in-line with a record early-melt season event, which combined with low snow accumulation

630 (Tedesco and Fettweis, 2020), promoted rapid snowpack warming, disintegration and exposure of the bare ice zone, resulting

in an enhanced melt-albedo feedback mechanism (Tedesco and Fettweis, 2020). Similar findings by Turton et al. (2021) and

Hochreuther et al. (2021) at 79°N Glacier recorded the largest SGL numbers and extents of their study periods in 2019,

indicating the widespread impact of this extreme melt event, particularly across the GrIS northern sector.

635 Similar seasonal and multi-annual behavioural patterns during 2017 and 2018 were, again, also observed by Turton et al.

(2021) and Lu et al. (2021) on the north-eastern glacier of 79°N and Otto et al. (2022) on the northern Ryder Glacier. These

findings all record a slow rate of SGL increase and late area peak (early-August) in 2017 and 2018, with Lu et al. (2021)

confirming the late area peak in combined supraglacial drainage mapping of both lakes and rivers during August 2017. SGL

mapping by Turton et al. (2021) also identified the delayed development and lower SGL presence during the 2018 melt season,

640 with SGLs largely limited to <900 m a.s.l. Such findings are consistent with observations in this study, with the onset and

inland evolution of the supraglacial network, including both rivers and lakes, delayed by ~1 month compared to other the other

study years (2016, 2019, 2020) and the limited areal development of the network (<1150 m a.s.l). Both the melt seasons of

2017 and 2018 recorded below average melt (1981 – 2010 reference period) and melt extents (32.9% and 44% respectively)

across the GrIS (Tedesco et al., 2017, 2018; Sasgen et al., 2020). There was heavy springtime snowfall and late surviving snow

645 in bare ice areas (Tedesco et al., 2017, 2018); consistent with a strongly positive average summer (JJA) North Atlantic

Oscillation and a negative Greenland Blocking Index, hypothesised to inhibit surface melt and promote increased summertime

snowfall (Ruan et al., 2019; Sasgen et al., 2020), hence these anomalously cold summers.

The anomalously early spike in satellite-derived meltwater area recorded in early-June 2020 raises questions as to how extreme

650 melt years, such as 2019, may precondition the ice surface (Cullather et al., 2020) and affect surface conditions and subsequent

surface hydrologic behaviour the following year (Culberg et al., 2021). Some SGLs on the GrIS have been found to persist

throughout the winter months, due to insulation from a layer of ice and/or snow (Koenig et al., 2015; Law et al., 2020; Schröder

et al., 2020). This lake persistence includes the winter of 2019/2020, when late-summer surface melt and high autumnal

temperatures (August – November) are believed to have increased subsurface firn temperatures, delaying and even decreasing

655 the ability for subsurface meltwater freezing in northern Greenland, contributing to higher totals of liquid-buried SGLs

(Dunmire et al., 2020). This alongside a drier-than-average (1981 – 2020) winter and spring (Tedesco and Fettweis, 2020;

Moon et al., 2020), has the potential to cause the rapid disintegration of limited snow present and the subsequent swift exposure

of the bare ice zone the following summer. This swift exposure would also include that of perennial rivers and lakes, much earlier in the melt season than expected, hence the increased MF value observed in this study despite low MAR-derived melt
660 production and runoff values.

5.3 Satellite-derived MF and runoff simulations

We found a positive linear relationship between satellite-derived MF and MAR simulated R before runoff declined (Fig. 6), showing how the MF-R relationship can be used to reliably simulate seasonal surface meltwater variation and provide further understanding into how runoff is routed and stored, at least up to peak melt events. This finding supports other studies that
665 have used satellite-derived meltwater metrics and RCM-modelled runoff which have focussed on the southwest GrIS (Yang et al., 2021), Northern GrIS (Lu et al., 2021; Li et al., 2022) and the Devon Ice Cap (Lu et al., 2020). In terms of post-peak melt events, surface meltwater can still cover a substantially large area even after surface runoff has reduced and ceased, as seen in this study. This is known as the 'delay' effect (Lu et al., 2021), whereby meltwater may continue to be routed or stored on the ice surface via the slow routing of melt out of snowpack/firn at higher elevations, the stagnation and subsequent
670 preservation of transported meltwater in large supraglacial rivers or the storage of melt in SGLs. Therefore, whilst this MF-R relationship is promising in providing comparative assessments between satellite observations and RCM-modelled runoff at HG, calculated runoff volume via satellite- (Yang et al., 2021) or field-based measurements (Smith et al., 2017) are required to provide further validation of such relationships, in particular over space and time across a full melt season.

5.4 Future implications

675 Substantial changes have taken place at HG over the last two decades driven by atmospheric and oceanic change (Carr et al., 2015; Rignot et al., 2021). It is therefore important to consider HG and the overall northern regions sensitivity to such warming under present climate scenarios. Northern Greenland is expected to undergo the greatest warming of the 21st Century across the GrIS (Hill et al., 2017), and given its already low rates of winter accumulation compared to other ice sheet sectors (Goelzer et al., 2013), means this region is likely to become ever more sensitive to climatic change in the future. Mapping performed
680 within this study illustrates the multi-annual persistence of the supraglacial drainage network within this high latitudinal region (Fig. 3a) and the rapid and extensive response of this system to high melt years (Fig. 4). This response, in particular to the extreme melt year of 2019, can precondition the ice surface for the following melt season, resulting in earlier but widespread hydrologic activity and longer-lasting melt season. This preconditioning and subsequent behaviour is likely to become increasingly normalised as melt events and atmospheric variability, such as persistent blocking events, increase in frequency
685 and intensity (Rahmstorf and Coumou, 2011; McLeod and Mote, 2016).

Inland migration of the supraglacial drainage network is also projected with continued warming (Leeson et al., 2015), with recent work already showing ablation area expansion and amplification of melt and runoff post-1990 across Northern Greenland (Noël et al., 2019). Many more surface depressions for future SGL locations are present above the current northern

690 ELA (Igneczi et al. 2016), with the potential to accumulate high volumes of meltwater and feed lengthening overflow supraglacial rivers that extend tens of kilometres downstream to non-local, low elevation moulins (Poinar et al., 2015). For ponded water, if ice becomes thin enough (Poinar et al., 2015), or localised ice columns become vulnerable to fracture from refrozen ice complexities within firn (ice-blobs; Culberg et al., 2022) new hydrofracture events will bring such meltwater to isolated areas of the ice sheet bed. This could have knock-on impacts to ice flow, with the likely delivery of water and heat to

695 a persistent inefficient subglacial system, where thicker, flatter ice may prohibit the development of an efficient subglacial system (Dow et al., 2014), enhancing ice flow (Christoffersen et al., 2018).

Persistent low-permeability ice slabs which block vertical percolation have continued to thicken overtime in the lower accumulation zone. Ice slabs are expected to enhance runoff from Greenland's interior, particularly in consecutive warm

700 summers (MacFerrin et al., 2019). Enhanced runoff and inland expansion of the supraglacial drainage network will impact meltwater feedback processes, not only in driving overall SMB decline (Noël et al., 2021) but further impacting dynamical behaviour, including hydrofracture potential. At HG, a particular concern is the vulnerability of its northern terminus to increased hydrofracture events from greater melt runoff (Carr et al., 2015). Such events at HG have the potential to promote future rapid run-away retreat of HG, especially if the northern sector of the terminus retreats beyond its pinning point into the

705 deepened bed (below sea level) in which is sits (Carr et al., 2015, Hillebrand et al., 2022).

As the northern region mainly consists of fast-flowing, marine-terminating outlet glaciers, like HG, that drain a large proportion of the GrIS, further understanding of the mechanisms that drive their dynamical behaviour, in particular related to enhanced runoff, are required for predicting their future contribution to GrIS mass loss and subsequent sea level rise.

710 **6 Conclusion**

In this study, we mapped and quantified for the first time, the spatial and temporal evolution of the supraglacial drainage network, including both rivers and lakes, using 10 m Sentinel-2 images from the melt seasons of 2016 to 2020 at Humboldt Glacier, northern Greenland. We identify an extensive supraglacial drainage network exists at Humboldt Glacier that is particularly prevalent up to 1000 m a.s.l with a further variable transient zone extending up to 1500 m a.s.l. The seasonal

715 evolutionary behaviour of this network migrates up-glacier in response to increasing runoff as air temperatures rise throughout the melt season, with the network transforming from an inefficient system dominated by water percolation and slush flows to one dominated by channelised, efficient flow. Interannual variability of the extent and behaviour of the system is associated with high and low melt years across the study period, with the low melt years of 2017 and 2018 having both limited and delayed spatial development. The extreme melt year of 2019 showed the extensive development and persistence of the

720 supraglacial drainage network into September, which followed by low snow accumulation during the subsequent winter/spring, preconditioned the ice sheet for earlier hydrologic activity in 2020; behaviour which may become more representative with

extreme melt events and longer-lasting melt seasons into the future. This work ultimately contributes to advancing our understanding of supraglacial hydrologic processes across the Greenland Ice Sheet by expanding detailed drainage mapping to other understudied regions of the ice sheet, in particular to Greenland's rapidly changing northern region, aiding in

725   projections of future mass loss as enhanced runoff continues with climatic warming.

7 Data Availability

Supraglacial river and lake shapefiles can be requested by contacting the lead author. Regional climate model MAR v3.11 data was provided by Dr Xavier Fettweis and is freely available via ftp://ftp.climato.be/ . Sentinel-2 imagery is available from the

730   Copernicus Open Access Hub (https://scihub.copernicus.eu) and digital elevation model ArcticDEM is available via https://www.pgc.umn.edu/data/arcticdem/.   The automatic river detection algorithm is freely available via https://github.com/njuRS/River_detection.

8 Supplementary Information

Supplementary data related to this article is available to view in the associated PDF.

735   9 Author Contributions

LDR designed the study, conducted data collection and analysis and prepared the manuscript. KY provided the source code for the automatic detection algorithm for automatic river mapping in Matlab. AJS aided with MAR data extraction for the Humboldt Glacier catchment. DMR, AJS, SJL and KY provided comments on draft versions of the manuscript produced by LDR.

740   10 Competing interests

Kang Yang is a member of the editorial board of The Cryosphere. The author(s) declare no other conflicts of interest.

11 Acknowledgements

LDR acknowledges financial support from a Natural Environmental Research Council (NERC) Doctoral Training Partnership (Grant number NE/L002450/1). Authors would like to acknowledge the Copernicus Open Access Hub for free access to the
745   satellite imagery used in this study and also thank Dr Xavier Fettweis for the availability of MAR data. We also thank the Polar Geospatial Center for availability of the ArcticDEM.

12 Financial Support

This research has been supported by the Natural Environment Research Council (NERC) Doctoral Training Partnership (Grant number NE/L002450/1).

750

References

Andrews, L. C., Catania, G. A., Hoffman, M. J., Gulley, J. D., Lüthi, M. P., Ryser, C., Hawley, R. L., and Neumann, T. A.: Direct observations of evolving subglacial drainage beneath the Greenland Ice Sheet, Nature, 514, 80-83, https://doi.org/10.1038/nature13796, 2014.

755 Andrews, L. C., Poinar, K., and Trunz, C.: Controls on Greenland moulin geometry and evolution from the Moulin Shape model, The Cryosphere, 16, 2421-2448, https://doi.org/10.5194/tc-16-2421-2022, 2022.

Baillarin, S., Meygret, A., Dechoz, C., Petrucci, B., Lacherade, S., Trémas, T., Isola, C., Martimort, P., and Spoto, F.: Sentinel-2 level 1 products and image processing performances, 2012 IEEE international geoscience and remote sensing symposium, 7003-7006, doi: https://doi.org/10.1109/IGARSS.2012.6351959, 2012.

760 Bartholomew, I., Nienow, P., Mair, D., Hubbard, A., King, M. A., and Sole, A.: Seasonal evolution of subglacial drainage and acceleration in a Greenland outlet glacier, Nature Geoscience, 3, 408-411, https://doi.org/10.1038/ngeo863, 2010.

Bartholomew, I., Nienow, P., Sole, A., Mair, D., Cowton, T., and King, M. A.: Short-term variability in Greenland Ice Sheet motion forced by time-varying meltwater drainage: Implications for the relationship between subglacial drainage system behavior and ice velocity, Journal of Geophysical Research: Earth Surface, 117, https://doi.org/10.1029/2011JF002220, 2012.

765 Box, J. E. and Decker, D. T.: Greenland marine-terminating glacier area changes: 2000–2010, Annals of Glaciology, 52, 91-98, https://doi.org/10.3189/172756411799096312, 2011.

Carr, J. R., Vieli, A., Stokes, C., Jamieson, S., Palmer, S., Christoffersen, P., Dowdeswell, J., Nick, F., Blankenship, D., and Young, D.: Basal topographic controls on rapid retreat of Humboldt Glacier, northern Greenland, Journal of Glaciology, 61, 137-150, https://doi.org/10.3189/2015JoG14J128, 2015.

770 Catania, G. A., Neumann, T. A., and Price, S. F.: Characterizing englacial drainage in the ablation zone of the Greenland ice sheet, Journal of Glaciology, 54, 567-578, https://doi.org/10.3189/002214308786570854, 2008.

Christoffersen, P., Bougamont, M., Hubbard, A., Doyle, S. H., Grigsby, S., and Pettersson, R.: Cascading lake drainage on the Greenland Ice Sheet triggered by tensile shock and fracture, Nature Communications, 9, 1064, https://doi.org/10.1038/s41467-018-03420-8, 2018.

775 Chu, V. W.: Greenland ice sheet hydrology: A review, Progress in Physical Geography, 38, 19-54, https://doi.org/10.1177/0309133313507075, 2014.

Crozier, J., Karlstrom, L., and Yang, K.: Basal control of supraglacial meltwater catchments<? xmltex\break?> on the Greenland Ice Sheet, The Cryosphere, 12, 3383-3407, https://doi.org/10.5194/tc-12-3383-2018, 2018.

Cuffey, K. M. and Paterson, W. S. B.: The physics of glaciers, Academic Press, 2010.

780   Culberg, R., Chu, W., and Schroeder, D. M.: Shallow Fracture Buffers High Elevation Runoff in Northwest Greenland, Geophysical Research Letters, doi: https://doi.org/10.1029/2022GL101151, 2022. e2022GL101151, https://doi.org/10.1029/2022GL101151, 2022.

Culberg, R., Schroeder, D. M., and Chu, W.: Extreme melt season ice layers reduce firn permeability across Greenland, Nature communications, 12, 2336, https://doi.org/10.1038/s41467-021-22656-5, 2021.

785   Cullather, R. I., Andrews, L. C., Croteau, M. J., Digirolamo, N. E., Hall, D. K., Lim, Y. K., Loomis, B. D., Shuman, C. A., and Nowicki, S. M.: Anomalous circulation in July 2019 resulting in mass loss on the Greenland Ice Sheet, Geophysical Research Letters, 47, e2020GL087263, https://doi.org/10.1029/2020GL087263, 2020.

Davison, B. J., Sole, A. J., Livingstone, S. J., Cowton, T. R., and Nienow, P. W.: The influence of hydrology on the dynamics of land-terminating sectors of the Greenland ice sheet, Frontiers in Earth Science, 7, 10, https://doi.org/10.3389/feart.2019.00010, 2019.

790   Dow, C., Kulessa, B., Rutt, I., Doyle, S. H., and Hubbard, A.: Upper bounds on subglacial channel development for interior regions of the Greenland ice sheet, Journal of Glaciology, 60, 1044-1052, https://doi.org/10.3189/2014JoG14J093, 2014.

Dunmire, D., Banwell, A. F., Wever, N., Lenaerts, J., and Datta, R. T.: Contrasting regional variability of buried meltwater extent over 2 years across the Greenland Ice Sheet, The Cryosphere, 15, 2983-3005, https://doi.org/10.5194/tc-15-2983-2021, 2021.

795   Elmes, A., Levy, C., Erb, A., Hall, D. K., Scambos, T. A., DiGirolamo, N., and Schaaf, C.: Consequences of the 2019 greenland ice sheet melt episode on albedo, Remote Sensing, 13, 227, https://doi.org/10.3390/rs13020227, 2021.

Gardner, A. S., M. A. Fahnestock, and T. A. Scambos., ITS_LIVE Regional Glacier and Ice Sheet Surface Velocities. Data archived at National Snow and Ice Data Center, https://doi.org/10.5067/6II6VW8LLWJ7, 2019.

800   Gleason, C. J., Smith, L. C., Chu, V. W., Legleiter, C. J., Pitcher, L. H., Overstreet, B. T., Rennermalm, A. K., Forster, R. R., and Yang, K.: Characterizing supraglacial meltwater channel hydraulics on the Greenland Ice Sheet from in situ observations, Earth Surface Processes and Landforms, 41, 2111-2122, https://doi.org/10.1002/esp.3977, 2016.

Gleason, C. J., Yang, K., Feng, D., Smith, L. C., Liu, K., Pitcher, L. H., Chu, V. W., Cooper, M. G., Overstreet, B. T., and Rennermalm, A. K.: Hourly surface meltwater routing for a Greenlandic supraglacial catchment across hillslopes and through
805   a dense topological channel network, The Cryosphere, 15, 2315-2331, https://doi.org/10.5194/tc-15-2315-2021, 2021.

Gledhill, L. A. and Williamson, A. G.: Inland advance of supraglacial lakes in north-west Greenland under recent climatic warming, Annals of Glaciology, 59, 66-82, https://doi.org/10.1017/aog.2017.31, 2018.

Goelzer, H., Huybrechts, P., Fürst, J. J., Nick, F. M., Andersen, M. L., Edwards, T. L., Fettweis, X., Payne, A. J., and Shannon, S.: Sensitivity of Greenland ice sheet projections to model formulations, Journal of Glaciology, 59, 733-749,
810   https://doi.org/10.3189/2013JoG12J182, 2013.

Gray, L.: Brief communication: Glacier run-off estimation using altimetry-derived basin volume change: case study at Humboldt Glacier, northwest Greenland, The Cryosphere, 15, 1005-1014, https://doi.org/10.5194/tc-15-1005-2021, 2021.

Greuell, W. and Knap, W. H.: Remote sensing of the albedo and detection of the slush line on the Greenland ice sheet, Journal of Geophysical Research: Atmospheres, 105, 15567-15576, https://doi.org/10.1029/1999JD901162, 2000.

815 Gudmundsson, G. H.: Transmission of basal variability to a glacier surface, Journal of Geophysical Research: Solid Earth, 108, https://doi.org/10.1029/2002JB002107, 2003.

Gudmundsson, G. H., Raymond, C. F., and Bindschadler, R.: The origin and longevity of flow stripes on Antarctic ice streams, Annals of Glaciology, 27, 145-152, https://doi.org/10.3189/1998AoG27-1-145-152, 1998.

Hanna, E., Cappelen, J., Fettweis, X., Mernild, S. H., Mote, T. L., Mottram, R., Steffen, K., Ballinger, T. J., and Hall, R. J.:

820 Greenland surface air temperature changes from 1981 to 2019 and implications for ice-sheet melt and mass-balance change, International Journal of Climatology, 41, E1336-E1352, https://doi.org/10.1002/joc.6771, 2021.

Hanna, E., Mernild, S. H., Cappelen, J., and Steffen, K.: Recent warming in Greenland in a long-term instrumental (1881–2012) climatic context: I. Evaluation of surface air temperature records, Environmental Research Letters, 7, 045404, https://doi.org/10.1088/1748-9326/7/4/045404, 2012.

825 Haran, T., J. Bohlander, T. Scambos, T. Painter, and M. Fahnestock. MEaSUREs MODIS Mosaic of Greenland (MOG) 2005, 2010, and 2015 Image Maps, Version 2. Boulder, Colorado USA. NASA National Snow and Ice Data Center Distributed Active Archive Center. https://doi.org/10.5067/9ZO79PHOTYE5, 2018, last access 21st November 2022.

Haran, T., J. Bohlander, T. Scambos, T. Painter, and M. Fahnestock. MEaSUREs MODIS Mosaic of Greenland 2005 (MOG2005) Image Map, Version 1. Boulder, Colorado. NSIDC: National Snow and Ice Data Center,

830 http://.doi.org/10.5067/IAGYM8Q26QRE, 2013.

Hill, E. A., Carr, J. R., and Stokes, C. R.: A review of recent changes in major marine-terminating outlet glaciers in Northern Greenland, Frontiers in Earth Science, 4, 111, https://doi.org/10.3389/feart.2016.00111, 2017.

Hill, E. A., Carr, J. R., Stokes, C. R., and Gudmundsson, G. H.: Dynamic changes in outlet glaciers in northern Greenland from 1948 to 2015, The Cryosphere, 12, 3243-3263, https://doi.org/10.5194/tc-12-3243-2018, 2018.

835 Hillebrand, T. R., Hoffman, M. J., Perego, M., Price, S. F., and Howat, I. M.: The contribution of Humboldt Glacier, North Greenland, to sea-level rise through 2100 constrained by recent observations of speedup and retreat, The Cryosphere, The Cryosphere, 16(11), 4679-4700, https://doi.org/10.5194/tc-16-4679-2022, 2022.

Hochreuther, P., Neckel, N., Reimann, N., Humbert, A., and Braun, M.: Fully automated detection of supraglacial lake area for Northeast Greenland using sentinel-2 time-series, Remote Sensing, 13, 205, https://doi.org/10.3390/rs13020205, 2021.

840 Hoffman, M., Catania, G., Neumann, T., Andrews, L., and Rumrill, J.: Links between acceleration, melting, and supraglacial lake drainage of the western Greenland Ice Sheet, Journal of Geophysical Research: Earth Surface, 116, https://doi.org/10.1029/2010JF001934, 2011.

Ignéczi, Á., Sole, A. J., Livingstone, S. J., Leeson, A. A., Fettweis, X., Selmes, N., Gourmelen, N., and Briggs, K.: Northeast sector of the Greenland Ice Sheet to undergo the greatest inland expansion of supraglacial lakes during the 21st century,

845 Geophysical Research Letters, 43, 9729-9738, https://doi.org/10.1002/2016GL070338, 2016.

Ignéczi, Á., Sole, A. J., Livingstone, S. J., Ng, F. S., and Yang, K.: Greenland Ice Sheet surface topography and drainage structure controlled by the transfer of basal variability, Frontiers in Earth Science, 6, 101, https://doi.org/10.3389/feart.2018.00101, 2018.

Irvine-Fynn, T. D., Hodson, A. J., Moorman, B. J., Vatne, G., and Hubbard, A. L.: Polythermal glacier hydrology: A review,
850   Reviews of Geophysics, 49, https://doi.org/10.1029/2010RG000350, 2011.

Joughin, I., Das, S., Flowers, G., Behn, M., Alley, R., King, M., Smith, B., Bamber, J., van den Broeke, M., and van Angelen, J.: Influence of supraglacial lakes and ice-sheet geometry on seasonal ice-flow variability, Cryosphere, 7, 1185-1192, https://doi.org/10.5194/tcd-7-1101-2013, 2013.

Joughin, I., Fahnestock, M., Kwok, R., Gogineni, P., and Allen, C.: Ice flow in the Humboldt, Petermann, and Ryder Glaciers,
855   North Greenland, Journal of Glaciology, 45, 231-341, https://doi.org/10.3189/S0022143000001738, 1999.

Joughin, I., Kwok, R., and Fahnestock, M.: Estimation of ice-sheet motion using satellite radar interferometry: method and error analysis with application to Humboldt Glacier, Greenland, Journal of Glaciology, 42, 564-575, https://doi.org/10.3189/S0022143000003543, 1996.

Kamb, B.: Glacier surge mechanism based on linked cavity configuration of the basal water conduit system, Journal of
860   Geophysical Research: Solid Earth, 92, 9083-9100, https://doi.org/10.1029/JB092iB09p09083, 1987.

Karlstrom, L. and Yang, K.: Fluvial supraglacial landscape evolution on the Greenland Ice Sheet, Geophysical Research Letters, 43, 2683-2692, https://doi.org/10.1002/2016GL067697, 2016.

Koenig, L. S., Lampkin, D., Montgomery, L., Hamilton, S., Turrin, J., Joseph, C., Moutsafa, S., Panzer, B., Casey, K., and Paden, J. D.: Wintertime storage of water in buried supraglacial lakes across the Greenland Ice Sheet, The Cryosphere, 9,
865   1333-1342, https://doi.org/10.5194/tc-9-1333-2015, 2015.

Lampkin, D. and VanderBerg, J.: A preliminary investigation of the influence of basal and surface topography on supraglacial lake distribution near Jakobshavn Isbrae, western Greenland, Hydrological Processes, 25, 3347-3355, https://doi.org/10.1002/hyp.8170, 2011.

Lampkin, D. and VanderBerg, J.: Supraglacial melt channel networks in the Jakobshavn Isbræ region during the 2007 melt
870   season, Hydrological Processes, 28, 6038-6053, https://doi.org/10.1002/hyp.10085, 2014.

Law, R., Arnold, N., Benedek, C., Tedesco, M., Banwell, A., and Willis, I.: Over-winter persistence of supraglacial lakes on the Greenland Ice Sheet: results and insights from a new model, Journal of Glaciology, 66, 362-372, https://doi.org/10.1017/jog.2020.7, 2020.

Leeson, A., Shepherd, A., Briggs, K., Howat, I., Fettweis, X., Morlighem, M., and Rignot, E.: Supraglacial lakes on the
875   Greenland ice sheet advance inland under warming climate, Nature Climate Change, 5, 51-55, https://doi.org/10.1038/nclimate2463, 2015.

Li, Y., Yang, K., Gao, S., Smith, L. C., Fettweis, X., and Li, M.: Surface meltwater runoff routing through a coupled supraglacial-proglacial drainage system, Inglefield Land, northwest Greenland, International Journal of Applied Earth Observation and Geoinformation, 106, 102647, https://doi.org/10.1016/j.jag.2021.102647, 2022.

880 Lim, Y.-K., Schubert, S. D., Nowicki, S. M., Lee, J. N., Molod, A. M., Cullather, R. I., Zhao, B., and Velicogna, I.: Atmospheric summer teleconnections and Greenland Ice Sheet surface mass variations: Insights from MERRA-2, Environmental Research Letters, 11, 024002, https://doi.org/10.1088/1748-9326/11/2/024002, 2016.

Livingstone, S. J., Chu, W., Ely, J. C., and Kingslake, J.: Paleofluvial and subglacial channel networks beneath Humboldt Glacier, Greenland, Geology, 45, 551-554, https://doi.org/10.1130/G38860.1, 2017.

885 Lu, Y., Yang, K., Lu, X., Li, Y., Gao, S., Mao, W., and Li, M.: Response of supraglacial rivers and lakes to ice flow and surface melt on the northeast Greenland ice sheet during the 2017 melt season, Journal of Hydrology, 602, 126750, https://doi.org/10.1016/j.jhydrol.2021.126750, 2021.

Lu, Y., Yang, K., Lu, X., Smith, L. C., Sole, A. J., Livingstone, S. J., Fettweis, X., and Li, M.: Diverse supraglacial drainage patterns on the Devon ice Cap, Arctic Canada, Journal of Maps, 16, 834-846, https://doi.org/10.1080/17445647.2020.1838353,
890 2020.

MacFerrin, M., Machguth, H., As, D. v., Charalampidis, C., Stevens, C., Heilig, A., Vandecrux, B., Langen, P., Mottram, R., and Fettweis, X.: Rapid expansion of Greenland's low-permeability ice slabs, Nature, 573, 403-407, https://doi.org/10.1038/s41586-019-1550-3, 2019.

Marston, R. A.: Supraglacial stream dynamics on the Juneau Icefield, Annals of the Association of American Geographers,
895 73, 597-608, https://doi.org/10.1111/j.1467-8306.1983.tb01861.x, 1983.

McFeeters, S. K.: The use of the Normalized Difference Water Index (NDWI) in the delineation of open water features, International journal of remote sensing, 17, 1425-1432, https://doi.org/10.1080/01431169608948714, 1996.

McLeod, J. T. and Mote, T. L.: Linking interannual variability in extreme Greenland blocking episodes to the recent increase in summer melting across the Greenland ice sheet, International Journal of Climatology, 36, 1484-1499,
900 https://doi.org/10.1002/joc.4440, 2016.

Mejia, J., Gulley, J., Trunz, C., Covington, M. D., Bartholomaus, T., Breithaupt, C., Xie, S., and Dixon, T. H.: Moulin density controls the timing of peak pressurization within the Greenland Ice Sheet's subglacial drainage system, Geophysical Research Letters, 49, e2022GL100058, https://doi.org/10.1029/2022GL100058, 2022.

Moon, T. A., Tedesco, M., Box, J., Cappelen, J., Fausto, R., Fettweis, X., Korsgaard, N., Loomis, B., Mankoff, K., and Mote,
905 T.: Arctic Report Card 2020: Greenland Ice Sheet, https://doi.org/10.25923/ms78-g612, 2020.

Morlighem, M., Williams, C. N., Rignot, E., An, L., Arndt, J. E., Bamber, J. L., Catania, G., Chauché, N., Dowdeswell, J. A., and Dorschel, B.: BedMachine v3: Complete bed topography and ocean bathymetry mapping of Greenland from multibeam echo sounding combined with mass conservation, Geophysical research letters, 44, 11,051-011,061, https://doi.org/10.1002/2017GL074954, 2017.

910 Morlighem, M. et al. IceBridge BedMachine Greenland, Version 4. [Bed Topography]. Boulder, Colorado USA. NASA National Snow and Ice Data Center Distributed Active Archive Center. https://doi.org/10.5067/VLJ5YXKCNGXO, 2021, last access 30th February 2021.

Mouginot, J., Rignot, E., Bjørk, A. A., Van den Broeke, M., Millan, R., Morlighem, M., Noël, B., Scheuchl, B., and Wood, M.: Forty-six years of Greenland Ice Sheet mass balance from 1972 to 2018, Proceedings of the national academy of sciences, 915   116, 9239-9244, https://doi.org/10.1073/pnas.1904242116, 2019.

Ng, F. S., Ignéczi, Á., Sole, A. J., and Livingstone, S. J.: Response of surface topography to basal variability along glacial flowlines, Journal of Geophysical Research: Earth Surface, 123, 2319-2340, https://doi.org/10.1029/2017JF004555, 2018.

Nienow, P., Sole, A., Slater, D. A., and Cowton, T.: Recent advances in our understanding of the role of meltwater in the Greenland Ice Sheet system, Current Climate Change Reports, 3, 330-344, https://doi.org/10.1007/s40641-017-0083-9, 2017.

920   Noël, B., van de Berg, W. J., Lhermitte, S., and van den Broeke, M. R.: Rapid ablation zone expansion amplifies north Greenland mass loss, Science advances, 5, eaaw0123, https://doi.org/10.1126/sciadv.aaw0123, 2019.

Oswald, G. K. and Gogineni, S.: Mapping basal melt under the northern Greenland Ice Sheet, IEEE Transactions on Geoscience and Remote Sensing, 50, 585-592, https://doi.org/10.1109/TGRS.2011.2162072., 2011.

Otto, J., Holmes, F. A., and Kirchner, N.: Supraglacial lake expansion, intensified lake drainage frequency, and first 925   observation of coupled lake drainage, during 1985–2020 at Ryder Glacier, Northern Greenland, Frontiers in Earth Science, 10, 978137, https://doi.org/10.3389/feart.2022.978137, 2022.

Pitcher, L. H. and Smith, L. C.: Supraglacial streams and rivers, Annual Review of Earth and Planetary Sciences, 47, 421-452, https://doi.org/10.1146/annurev-earth-053018-060212, 2019.

Poinar, K., Joughin, I., Das, S. B., Behn, M. D., Lenaerts, J. T., and Van Den Broeke, M. R.: Limits to future expansion of 930   surface-melt-enhanced ice flow into the interior of western Greenland, Geophysical Research Letters, 42, 1800-1807, https://doi.org/10.1002/2015GL063192, 2015.

Pope, A., Scambos, T. A., Moussavi, M., Tedesco, M., Willis, M., Shean, D., and Grigsby, S.: Estimating supraglacial lake depth in West Greenland using Landsat 8 and comparison with other multispectral methods, The Cryosphere, 10, 15-27, https://doi.org/10.5194/tc-10-15-2016, 2016.

935   Rahmstorf, S. and Coumou, D.: Increase of extreme events in a warming world, Proceedings of the National Academy of Sciences, 108, 17905-17909, https://doi.org/10.1073/pnas.1101766108, 2011.

Raymond, M. J. and Gudmundsson, G. H.: On the relationship between surface and basal properties on glaciers, ice sheets, and ice streams, Journal of Geophysical Research: Solid Earth, 110, https://doi.org/10.1029/2005JB003681, 2005.

Rennermalm, A. K., Smith, L. C., Chu, V., Box, J., Forster, R., Van den Broeke, M., Van As, D., and Moustafa, S. E.: Evidence 940   of meltwater retention within the Greenland ice sheet, The Cryosphere, 7, 1433-1445, https://doi.org/10.5194/tc-7-1433-2013, 2013.

Rignot, E., An, L., Chauche, N., Morlighem, M., Jeong, S., Wood, M., Mouginot, J., Willis, J. K., Klaucke, I., and Weinrebe, W.: Retreat of Humboldt Gletscher, North Greenland, driven by undercutting from a warmer ocean, Geophysical research letters, 48, e2020GL091342, https://doi.org/10.1029/2020GL091342, 2021.

945   Rignot, E. and Kanagaratnam, P.: Changes in the velocity structure of the Greenland Ice Sheet, Science, 311, 986-990, https://doi.org/10.1126/science.1121381, 2006.

Riihelä, A., King, M. D., and Anttila, K.: The surface albedo of the Greenland Ice Sheet between 1982 and 2015 from the CLARA-A2 dataset and its relationship to the ice sheet's surface mass balance, The Cryosphere, 13, 2597-2614, https://doi.org/10.5194/tc-13-2597-2019, 2019.

950 Rippin, D. and Rawlins, L.: Supraglacial River Networks, In International Encyclopedia of Geography (eds D. Richardson, N. Castree, M.F. Goodchild, A. Kobayashi, W. Liu and R.A. Marston), https://doi.org/10.1002/9781118786352.wbieg2072, 2021.

Ruan, R., Chen, X., Zhao, J., Perrie, W., Mottram, R., Zhang, M., Diao, Y., Du, L., and Wu, L.: Decelerated Greenland Ice Sheet melt driven by positive summer North Atlantic oscillation, Journal of Geophysical Research: Atmospheres, 124, 7633-

955 7646, https://doi.org/10.1029/2019JD030689, 2019.

Ryan, J., Smith, L., Van As, D., Cooley, S., Cooper, M., Pitcher, L., and Hubbard, A.: Greenland Ice Sheet surface melt amplified by snowline migration and bare ice exposure, Science Advances, 5, eaav3738, https://doi.org/10.1126/sciadv.aav3738, 2019.

Ryan, J. C., Hubbard, A., Stibal, M., Irvine-Fynn, T. D., Cook, J., Smith, L. C., Cameron, K., and Box, J.: Dark zone of the

960 Greenland Ice Sheet controlled by distributed biologically-active impurities, Nature communications, 9, 1065, https://doi.org/10.1038/s41467-018-03353-2, 2018.

Sasgen, I., Wouters, B., Gardner, A. S., King, M. D., Tedesco, M., Landerer, F. W., Dahle, C., Save, H., and Fettweis, X.: Return to rapid ice loss in Greenland and record loss in 2019 detected by the GRACE-FO satellites, Communications Earth & Environment, 1, 1-8, https://doi.org/10.1038/s43247-020-0010-1, 2020.

965 Schoof, C.: Ice-sheet acceleration driven by melt supply variability, Nature, 468, 803-806, https://doi.org/10.1038/nature09618, 2010.

Schröder, L., Neckel, N., Zindler, R., and Humbert, A.: Perennial supraglacial lakes in Northeast Greenland observed by polarimetric SAR, Remote Sensing, 12, 2798, https://doi.org/10.3390/rs12172798, 2020.

Selmes, N., Murray, T., and James, T.: Fast draining lakes on the Greenland Ice Sheet, Geophysical Research Letters, 38,

970 https://doi.org/10.1029/2011GL047872, 2011.

Slater, T., Shepherd, A., McMillan, M., Leeson, A., Gilbert, L., Muir, A., Munneke, P. K., Noël, B., Fettweis, X., and van den Broeke, M.: Increased variability in Greenland Ice Sheet runoff from satellite observations, Nature Communications, 12, 6069, https://doi.org/10.1038/s41467-021-26229-4, 2021.

Smith, L. C., Chu, V. W., Yang, K., Gleason, C. J., Pitcher, L. H., Rennermalm, A. K., Legleiter, C. J., Behar, A. E., Overstreet,

975 B. T., and Moustafa, S. E.: Efficient meltwater drainage through supraglacial streams and rivers on the southwest Greenland ice sheet, Proceedings of the National Academy of Sciences, 112, 1001-1006, https://doi.org/10.1073/pnas.1413024112, 2015.

Smith, L. C., Yang, K., Pitcher, L. H., Overstreet, B. T., Chu, V. W., Rennermalm, Å. K., Ryan, J. C., Cooper, M. G., Gleason, C. J., and Tedesco, M.: Direct measurements of meltwater runoff on the Greenland ice sheet surface, Proceedings of the National Academy of Sciences, 114, E10622-E10631, https://doi.org/10.1073/pnas.1707743114, 2017.

980   Sole, A. J., Mair, D. W. F., Nienow, P. W., Bartholomew, I., King, M., Burke, M. J., and Joughin, I.: Seasonal speedup of a Greenland marine-terminating outlet glacier forced by surface melt–induced changes in subglacial hydrology, Journal of Geophysical Research: Earth Surface, 116, https://doi.org/10.1029/2010JF001948, 2011.

Tedesco, M., Box, J.E., Capplelen, J., Fausto, R.S., Fettweis, X., Hansen, K., Mote, T., Sasgen, I., Smeets, C.J.P.P., van As, D., van de Wal, R.S.W., Velicogna, I. (2017) NOAA Arctic Report Card 2018: Greenland Ice Sheet in Arctic Report Card

985   2017. Available online: https://arctic.noaa.gov/Report-Card/Report-Card-2017, last access 20th November 2022.

Tedesco, M., Box, J.E., Capplelen, J., Fausto, R.S., Fettweis, X., Hansen, K., Mote, T., Sasgen, I., Smeets, C.J.P.P., van As, D., van de Wal, R.S.W., Velicogna, I. (2017) NOAA Arctic Report Card 2018: Greenland Ice Sheet in Arctic Report Card 2017. Available online: https://arctic.noaa.gov/Report-Card/Report-Card-2017, last access 20th November 2022.

Tedesco, M., Box, J.E., Cappelen, J., Fausto, R.S., Fettweis, X., Anderson, J.K., Mote, T., Smeets, C.J.P.P., van As, D., van

990   de Wal, R.S.W. (2018). NOAA Arctic Report Card 2018: Greenland Ice Sheet in Arctic Report Card 2018. Available online: https://arctic.noaa.gov/Report-Card/Report-Card-2018, last access 20th November 2022.

Tedesco, M., Doherty, S., Fettweis, X., Alexander, P., Jeyaratnam, J., and Stroeve, J.: The darkening of the Greenland ice sheet: trends, drivers, and projections (1981–2100), The Cryosphere, 10, 477-496, https://doi.org/10.5194/tc-10-477-2016, 2016.

995   Tedesco, M. and Fettweis, X.: Unprecedented atmospheric conditions (1948–2019) drive the 2019 exceptional melting season over the Greenland ice sheet, The Cryosphere, 14, 1209-1223, https://doi.org/10.5194/tc-14-1209-2020, 2020.

Tedesco, M., Moon, T., Anderson, J.K., Box, J.E., Cappelen, J., Fausto, R.S., Fettweis, X., Loomis, B., Mankoff, K.D., Mote, T., Smeets, C.J.P.P., van As, D., van de Wal, R.S.W. Greenland Ice Sheet in Arctic Report Card 2019; Available online: https://arctic.noaa.gov/Report-Card/Report-Card-2019, last access 21st November 2022

1000   The IMBIE Team.: Mass balance of the Greenland Ice Sheet from 1992 to 2018, Nature, 579, 233-239, https://doi.org/10.1038/s41586-019-1855-2, 2020.

Trusel, L. D., Das, S. B., Osman, M. B., Evans, M. J., Smith, B. E., Fettweis, X., McConnell, J. R., Noël, B. P., and van den Broeke, M. R.: Nonlinear rise in Greenland runoff in response to post-industrial Arctic warming, Nature, 564, 104-108, https://doi.org/10.1038/s41586-018-0752-4, 2018.

1005   Turton, J. V., Hochreuther, P., Reimann, N., and Blau, M. T.: The distribution and evolution of supraglacial lakes on 79 N Glacier (north-eastern Greenland) and interannual climatic controls, The Cryosphere, 15, 3877-3896, https://doi.org/10.5194/tc-15-3877-2021, 2021.

van den Broeke, M., Box, J., Fettweis, X., Hanna, E., Noël, B., Tedesco, M., van As, D., van de Berg, W. J., and van Kampenhout, L.: Greenland ice sheet surface mass loss: recent developments in observation and modeling, Current Climate

1010   Change Reports, 3, 345-356, https://doi.org/10.1007/s40641-017-0084-8, 2017.

Van den Broeke, M. R., Enderlin, E. M., Howat, I. M., Kuipers Munneke, P., Noël, B. P., Van De Berg, W. J., Van Meijgaard, E., and Wouters, B.: On the recent contribution of the Greenland ice sheet to sea level change, The Cryosphere, 10, 1933-1946, https://doi.org/10.5194/tc-10-1933-2016, 2016.

Williamson, A. G., Arnold, N. S., Banwell, A. F., and Willis, I. C.: A Fully Automated Supraglacial lake area and volume Tracking ("FAST") algorithm: Development and application using MODIS imagery of West Greenland, Remote Sensing of Environment, 196, 113-133, https://doi.org/10.1016/j.rse.2017.04.032, 2017.

Williamson, A. G., Banwell, A. F., Willis, I. C., and Arnold, N. S.: Dual-satellite (Sentinel-2 and Landsat 8) remote sensing of supraglacial lakes in Greenland, The Cryosphere, 12, 3045-3065, https://doi.org/10.5194/tc-12-3045-2018, 2018.

Wyatt, F. R. and Sharp, M. J.: Linking surface hydrology to flow regimes and patterns of velocity variability on Devon Ice Cap, Nunavut, Journal of Glaciology, 61, 387-399, https://doi.org/10.3189/2015JoG14J109, 2015.

Yang, K. and Smith, L. C.: Supraglacial streams on the Greenland Ice Sheet delineated from combined spectral–shape information in high-resolution satellite imagery, IEEE Geoscience and Remote Sensing Letters, 10, 801-805, https://doi.org/10.1109/LGRS.2012.2224316., 2012.

Yang, K., Smith, L. C., Chu, V. W., Gleason, C. J., and Li, M.: A caution on the use of surface digital elevation models to simulate supraglacial hydrology of the Greenland ice sheet, IEEE Journal of Selected Topics in Applied Earth Observations and Remote Sensing, 8, 5212-5224, https://doi.org/10.1109/JSTARS.2015.2483483., 2015.

Yang, K., Smith, L. C., Cooper, M. G., Pitcher, L. H., Van As, D., Lu, Y., Lu, X., and Li, M.: Seasonal evolution of supraglacial lakes and rivers on the southwest Greenland Ice Sheet, Journal of Glaciology, 67, 592-602, https://doi.org/10.1017/jog.2021.10, 2021.

Yang, K., Smith, L. C., Sole, A., Livingstone, S. J., Cheng, X., Chen, Z., and Li, M.: Supraglacial rivers on the northwest Greenland Ice Sheet, Devon Ice Cap, and Barnes Ice Cap mapped using Sentinel-2 imagery, International Journal of Applied Earth Observation and Geoinformation, 78, 1-13, https://doi.org/10.1016/j.jag.2019.01.008, 2019a.

Yang, K., Smith, L. C., Fettweis, X., Gleason, C. J., Lu, Y., and Li, M.: Surface meltwater runoff on the Greenland ice sheet estimated from remotely sensed supraglacial lake infilling rate, Remote Sensing of Environment, 234, 111459, https://doi.org/10.1016/j.rse.2019.111459, 2019b.

Zhang, Q., Huai, B., van Den Broeke, M. R., Cappelen, J., Ding, M., Wang, Y., and Sun, W.: Temporal and Spatial Variability in Contemporary Greenland Warming (1958–2020), Journal of Climate, 35, 2755-2767, https://doi.org/10.1175/JCLI-D-21-0313.1, 2022.

Zwally, H. J., Abdalati, W., Herring, T., Larson, K., Saba, J., and Steffen, K.: Surface melt-induced acceleration of Greenland ice-sheet flow, Science, 297, 218-222, https://doi.org/10.1126/science.1072708, 2002.